

# GraphToxin: Reconstructing Full Unlearned Graphs from Graph Unlearning

Ying Song and Balaji Palanisamy

*University of Pittsburgh  
Pittsburgh, PA, USA*

**Abstract**—Graph unlearning has emerged as a promising solution for complying with “the right to be forgotten” regulations by enabling the removal of sensitive information upon request. However, this solution is not foolproof. The involvement of multiple parties creates new attack surfaces, and residual traces of deleted data can still remain in the unlearned graph neural networks (GNNs). These vulnerabilities can be exploited by attackers to recover the supposedly erased samples, thereby undermining the inherent functionality of graph unlearning.

In this work, we propose GraphToxin, the first graph reconstruction attack against graph unlearning. Specifically, we introduce a novel curvature matching module to provide a fine-grained guidance for full unlearned graph recovery. We demonstrate that GraphToxin can successfully subvert the regulatory guarantees expected from graph unlearning—it can recover not only a deleted individual’s information and personal links but also sensitive content from their connections, thereby posing substantially more detrimental threats. Furthermore, we extend GraphToxin to multiple node removal under both white-box and black-box setting, showcasing its practical feasibility and its potential to cause considerable harm.

We highlight the necessity of a worst-case analysis and propose a comprehensive evaluation framework to systematically assess the attack performance under both random and worst-case node removal scenarios. This provides a more robust and realistic measure of the vulnerability of graph unlearning methods to graph reconstruction attacks. Our extensive experiments demonstrate the effectiveness and flexibility of GraphToxin. Notably, we show that existing defense mechanisms are largely ineffective against this attack and, in some cases, can even amplify its performance. Given the severe privacy risks posed by GraphToxin, our work underscores the urgent need for the development of more effective and robust defense strategies against this type of attacks.

## 1. Introduction

Graph neural networks (GNNs) have demonstrated remarkable success across diverse domains, including social network analysis, drug discovery, and financial risk management. Their strength lies in capturing complex structural dependencies through iterative message passing. However, this mechanism inherently amplifies the risk of sensitive information leakage, raising significant user privacy concerns. Concurrently, data protection regulations such as the General Data Protection Regulation (GDPR) [1] enforce the “right to be forgotten”, requiring GNNs’ capacity to remove personal

data upon request. These privacy and legal imperatives have spurred the rapid emergence of graph unlearning (GU) [2].

Graph unlearning aims to scrub the influence of specific nodes, edges, or subgraphs from a trained GNN while preserving model performance on the remaining graph. Specifically, upon an unlearning request, the model owner typically employs parameter adjustments or gradient-based optimization to mitigate these effects instead of full retraining—which is prohibitively expensive and time-consuming—and subsequently releases the unlearned version. Despite its success, GU inevitably leaves residual traces of the “forgotten” targets. Although such remnants are often small enough to avoid noticeable degradation in overall performance, they can still be exploited by adversaries through membership inference [3] or graph reconstruction attacks, thereby undermining privacy guarantees. Moreover, the involvement of multiple parties further expands the attack surface. For instance, the service providers or platforms can retain copies of the previous models prior to unlearning while users can download such models locally on their devices. These decentralized behaviors fundamentally undermine the assurance of GU. In this work, we focus on the most challenging scenario—node unlearning [4] for node-level tasks—and present the first full graph reconstruction attack against graph unlearning (GU-FGRA).

**Research Gap—Graph Unlearning** To the best of our knowledge, only one prior work [3] has investigated the privacy risks of GU. However, their study is limited to a single edge removal and only aims to infer the link membership of a given node pair, rather than reconstructing the full deleted graph topology. Consequently, their approach solely reveals minimal information and fails to recover confidential or sensitive content encoded in node features. Additionally, their attack assumptions—access to partial unlearned/remaining graphs and a shadow graph with a distribution similar to that of the original graph—are unrealistic in practice due to strict security and privacy policies. Even if partial data were leaked, finding a faithful replica of the original dataset is infeasible and using publicly available data from a different distribution severely degrades the quality of reconstructed graphs due to distributional shifts.

**Graph Reconstruction Attack (GRA)** Regarding GRA, most existing studies primarily focus on inferring link memberships [5], [6]. Only a few attempt to recover sensitive node features [7], [8] or reconstruct the entire graph topology [9], [10]. This inconsistent terminology can be misleading, as a true full GRA should reveal all graph com-

ponents. Moreover, current research typically rely on access to node embeddings or shadow models, and often assume that sensitive node features or portions of the topology are available for recovery. They also lack comprehensive evaluation, hindering their practical applicability in scenarios such as red-teaming and model auditing.

**Machine Unlearning** Existing inversion attacks against MU cannot be trivially adapted to GU-FGRA, as the complex topological structures and rich node features in graphs produce entangled patterns during GNN message passing. To date, only one work [11] has explored single sample reconstruction in MU. However, it is limited to partial recovery of deleted samples under a white-box setting and performs poorly when targeting multiple deletions. Under the i.i.d. assumption, its multiple removals can be treated as a series of independent single removals. In contrast, graph unlearning is fundamentally different: due to the “ripple effects” propagated through GNNs, even a single node removal can affect its neighbors and higher-order structures, preventing a straightforward extension to GU.

**Research Questions** The above research gap motivates us to identify three key research questions in GU:

- 1) Is it possible to recover full unlearned graphs under realistic white-box settings and how this attack can be extended to multiple node removals?
- 2) Can this attack be generalized to the black-box setting and reconstruct full unlearned graphs using only minimal prior knowledge for multiple node removals?
- 3) How can we rigorously and comprehensively evaluate the performance of this full reconstruction attack?

**Unique Challenges and Strategies** Beyond the severe challenges previously discussed, the feasibility of gradient-based GU-FGRA under realistic attack settings remains underexplored. Since no shadow graphs or models are available and only minimal prior knowledge is mastered, even a simple unlearning attack targeting a single node is an intricate task. Notably, our goal is to reveal full unlearned graphs rather than a simple combination of multiple attribute inference attacks of the deleted node and multiple link membership inference attacks of its 1-hop neighbors. This challenge is further exacerbated for multiple node removals due to much worse structural and feature entanglements and ultimately more obscure gradient proxy for full graph recovery.

To answer the key research questions and to address their unique challenges under a realistic white-box setting, we present **GraphToxin, the first full graph reconstruction attack against graph unlearning**. Since the difference of publicly leaked gradients from the original GNN and its unlearned GNN implicitly encodes the information of the deleted graph, GraphToxin exploits this gradient difference for full graph recovery through three core modules. First, the gradient matching module acts as a holistic roadmap for full unlearned graph recovery by bridging the gap between the ground-truth gradient difference and gradients from the generated unlearned graph, however, it only yields a coarse proxy. Second, a novel curvature matching module provides fine-grained signals by penalizing the directions of high curvature to ultimately produce a more plausible recovery

solution. Finally, a feature smoothness module is utilized to capture and enforce similarity among connected nodes.

GraphToxin also tackles the intractable challenge of the data-free black-box setting. This scenario presents a major hurdle since attackers are restricted to using the model’s posterior probabilities only instead of its gradients. This limitation inevitably introduces approximation errors, as black-box GU-FGRA must attempt to infer fine-grained graph details from coarse posterior outputs, which can significantly degrade the reconstruction quality. To mitigate this issue, GraphToxin introduces a semantic calibration module. The goal of this module is to minimize the discrepancy between the ground-truth labels and the predictions for the recovered nodes, thereby improving the attack’s fidelity.

The efficacy of GraphToxin is validated through a rigorous and comprehensive evaluation framework. We contend that the conventional setting of our attack target is unconvincing as it focuses solely on small-scale random removals of the training graph [2], [12], [13], [14]. Given the inherent sparsity of real-world graphs, this operation often selects nodes that are less influential for model predictions. These “unimportant” nodes typically possess low degrees and cause negligible influences after removal. However, in reality, attackers would prioritize high-value targets. To better mimic actual attacks, we propose a worst-case unlearning analysis. In this research, we define this worst-case scenario as the removal of the top 10% of nodes with the highest degrees. Furthermore, we argue that existing evaluation metrics are often simplistic and unreliable [15], [16], [17]. Accordingly, we develop a systematic evaluation framework that incorporates reconstruction-related metrics to jointly measure both recovered features and topology from a global view, and performance-level metrics to assess the functional utility of the full recovered graph.

**Contribution** Our contributions are summarized as follows:

- 1) **Pioneering Attack:** We design GraphToxin, the first full graph reconstruction attack against graph unlearning. It not only recovers the deleted nodes and their graph topology, but also steals the sensitive information of their neighbors, posing more detrimental privacy risks.
- 2) **Novel Methodology:** We propose a novel curvature matching module to provide fine-grained guidance for full unlearned graph recovery in realistic settings.
- 3) **Scalability and Generalization:** We successfully extend GraphToxin to multiple node removals with comparable attack performance. We also generalize GraphToxin to the black-box setting with only minimal prior knowledge.
- 4) **Rigorous Evaluation Framework Design:** We propose a rigorous evaluation framework grounded in feature-level, global-level, and performance-level perspectives. We also investigate GraphToxin after removing the most influential nodes to assess its attack potency in reality.
- 5) **Empirical Validation:** We conduct extensive experiments across diverse graph datasets, GNN backbones, and both exact and approximate graph unlearning methods. The results demonstrate the effectiveness and flexibility of GraphToxin in both white-box and black-box settings, for a single or multiple node removals.

6) **Highlighting Urgency for Robust Defenses:** We empirically show that current defense methods fail to sufficiently mitigate or even enhance the attack performance of GraphToxin. This finding highlights the urgent need for developing more effective defense mechanisms against this potent attack.

**Social Impacts** GraphToxin is significantly more detrimental than existing inference attacks, particularly in high-stake scenarios, because it recovers not only an individual’s sensitive content and personal links, but also confidential information of her/his contacts. For instance, in financial crediting, revealing the full unlearned transaction graphs can expose private trades and confidential documents; in health-care management, reconstructing full health information can fuel workplace discrimination, insurance denial, or social stigma. Once privacy is undermined, the consequences are twofold: first, it can trigger a cascade of adversarial attacks, such as re-identification or model extraction; second, organizations face liability for non-compliance with regulations and simultaneously erode users’ trust in their AI systems.

## 2. Background and Problem Statement

### 2.1. Notations

Given an undirected attributed graph  $\mathcal{G} = (\mathcal{V}, \mathcal{E}, X)$ ,  $\mathcal{V}$  denotes the node set with cardinality  $|\mathcal{V}|$  and each node  $v$  is associated with a feature vector  $X_v \in \mathbb{R}^{1 \times \mathcal{D}}$  and a label vector  $Y_v \in \mathbb{R}^{1 \times |\mathcal{Y}|}$ , where  $\mathcal{D}$  is the feature dimension and  $|\mathcal{Y}|$  denotes the number of labels.  $\mathcal{E}$  denotes the set of edges with  $|\mathcal{E}|$  elements, which can be represented by an adjacency matrix  $A \in \{0, 1\}^{|\mathcal{V}| \times |\mathcal{V}|}$ , where  $A_{u,v} = 1$  iff  $(u, v) \in \mathcal{E}$ , and  $A_{u,v} = 0$  otherwise. For simplicity, we denote the graph as  $\mathcal{G} = (A, X)$ .  $\mathcal{F}_{ori}$ ,  $\mathcal{F}_{un}$  and  $\mathcal{F}_{att}$  indicate the original GNN, unlearned GNN, and GU-FGRA, respectively.

### 2.2. Graph Neural Networks

The exceptional performance of most GNNs stems from the message-passing mechanism, which aggregates information from each node  $v$ ’s local neighborhood  $\mathcal{N}(v)$  and iteratively updates the node embedding  $H_v^k$  after  $k$  layers. Formally, this process can be expressed as:

$$H_v^k = UPD^k(H_v^{k-1}, AGG^{k-1}(\{H_u^{k-1} : u \in \mathcal{N}(v)\})) \quad (1)$$

where  $H_v^0 = X_v$ , and  $UPD$  and  $AGG$  are two arbitrary differentiable functions to design diverse GNN variants. For node classification tasks, generally,  $H_v^k$  is fed into a linear classifier with a softmax function for final prediction.

### 2.3. Graph Unlearning

We only consider the most challenging GU—node unlearning throughout our paper, which is formally defined as:

**Definition 1 (Single Node Unlearning).** Given the original training graph  $\mathcal{G} = (A, X)$ , the original trained GNN  $\mathcal{F}_{ori}$

and a specific unlearning request  $\Delta\mathcal{G}_v = (v, \mathcal{E}_{\mathcal{N}_v^1}, X_v)$ , node unlearning aims to unlearn a single node  $v$ , its feature  $X_v$  and its links to 1-hop neighbors  $\mathcal{N}_v^1$  while minimizing the discrepancy between the unlearned model  $\mathcal{F}_{un_{\Delta\mathcal{G}_v}}$  and the fully retrained model  $\mathcal{F}_{\mathcal{G} \setminus \Delta\mathcal{G}_v}$ .

**Definition 2 (Multiple Node Unlearning).** Upon multiple unlearning requests  $\Delta\mathcal{G} = (\mathcal{V}_d, \mathcal{E}_d, X_d)$ , node unlearning aims to unlearn multiple nodes  $\mathcal{V}_d$ , their node features  $X_d$  and links to their 1-hop neighbors  $\mathcal{E}_d$ , while minimizing the discrepancy between the unlearned model  $\mathcal{F}_{un_{\Delta\mathcal{G}}}$  and the fully retrained model  $\mathcal{F}_{\mathcal{G} \setminus \Delta\mathcal{G}}$ . Different from single node unlearning,  $\mathcal{E}_d$  is much more complicated rather than a simple combination of multiple  $\mathcal{N}_v^1, v \in \mathcal{V}_d$ .

## 2.4. Graph Reconstruction Attack (GRA)

**Definition 3 (General GRA).** Given a trained GNN  $\mathcal{F}$  and attack knowledge  $\mathcal{K}$ , GRA  $\mathcal{F}^{-1}$  endeavors to recover sensitive information  $\mathcal{G}_{par}$  of its training graph  $\mathcal{G}$  by minimizing the distance between the reconstructed component  $\hat{\mathcal{G}}_{par}$  and its ground-truth  $\mathcal{G}_{par}$ , where  $\hat{\mathcal{G}}_{par} = \mathcal{F}^{-1}(\mathcal{K})$  and  $\mathcal{G}_{par} \in \mathcal{G}$ .

Based on the type of  $\mathcal{K}$ , general GRA can be specialized to white-box GRA when  $\mathcal{K}$  contains model gradients  $\nabla\mathcal{L}(\theta)$  (where  $\theta$  represents model parameters); it transforms into gray-box GRA when  $\mathcal{K}$  covers node embeddings but no white-box knowledge; and it presents black-box GRA when none of the above information is available.

Based on the recovered information  $\hat{\mathcal{G}}_{par}$ , general GRA can target specific components: recovering partial or full node features through attribute inference attacks, inferring a specific link membership via link stealing attacks, or reconstructing topological structures through graph topology reconstruction attacks. Our research tackles the most challenging objective—fully revealing node features and graph topology of unlearned graphs through full GRA. We provide a clear comparison of these attacks in Table 1.

## 2.5. Problem Statement

We formally define the full graph reconstruction attack against graph unlearning (GU-FGRA) as follows. Specifically, for a single node removal, attackers aim to identify the optimal attack model  $\mathcal{F}_{att_{\Delta\mathcal{G}_v}} = {}^*\mathcal{F}_{\Delta\mathcal{G}_v}^{-1}(\Delta\nabla\mathcal{L}(\theta_{\Delta\mathcal{G}_v}))$  to recover the full unlearned graph  $\mathcal{G}_{d_v}$ , where  $\Delta\nabla\mathcal{L}(\theta_{\Delta\mathcal{G}_v})$  denotes the difference between the gradients of the original and unlearned models ( $\nabla\mathcal{L}(\theta_{ori})$  and  $\nabla\mathcal{L}(\theta_{un_{\Delta\mathcal{G}_v}})$ ), and  $\mathcal{L}$  represents the empirical risk function.  $\mathcal{G}_{d_v} = (\mathcal{V}_{rec_v}, \mathcal{E}_{\mathcal{N}_v^1}, \mathcal{X}_{rec_v})$ , where recovery nodes  $\mathcal{V}_{rec_v} = [v, \mathcal{N}_v^1]$  contain the deleted node  $v$  and its affected 1-hop neighbors  $\mathcal{N}_v^1$ . Please note that  $\mathcal{G}_{d_v} \neq \Delta\mathcal{G}_v$  since there is no isolated node in  $\mathcal{G}$ ,  $|\mathcal{G}_{d_v}| > |\Delta\mathcal{G}_v|$ . Moreover, recovering  $\Delta\mathcal{G}_v$  can be simply treated as a combination of  $\mathcal{D}$  times attribute inference attacks of a single node  $v$  and a graph topology reconstruction attack of its associated links  $\mathcal{N}_v^1$  (i.e., a star graph). However, recovering  $\mathcal{G}_{d_v}$  is significantly more complicated, as it further requires the simultaneous full feature recovery

TABLE 1: **Attack Comparison.**  $\checkmark$  represents “access” or “applicable”,  $\times$  represents “no access”,  $\star$  denotes “shadow graph”, and  $\emptyset$  denotes “not applicable” or “unknown”. N/A means unexplored in the field.

Attack Type	Attack Knowledge $\mathcal{K}$			Recovery Content $\mathcal{G}_{par}$	Attack Unlearning Case				
	Graph Data	Model Access	Graph Unlearning			Feature	Topology	Random	Worse
Attribute Inference Attack (N/A)	$\checkmark^\star$	Grey/Black Box	$\emptyset$	Single/Partial	$\emptyset$	$\emptyset$	$\emptyset$	$\emptyset$	$\emptyset$
Link Stealing Attack [3]	$\checkmark^\star$	Grey/Black Box	Partial Unlearned Graph	$\emptyset$	Edge	$\checkmark$	$\emptyset$	$\emptyset$	$\emptyset$
Graph Topology Reconstruction Attack (N/A)	$\checkmark^\star$	Grey/Black Box	$\emptyset$	$\emptyset$	Partial/Full	$\emptyset$	$\emptyset$	$\emptyset$	$\emptyset$
Full Graph Reconstruction Attack (Ours)	$\times$	White/Grey/Black Box	Simple Unlearning Statistics	Full	Full	$\checkmark$	$\checkmark$	$\checkmark$	$\checkmark$

of multiple nodes. For multiple node removals, attackers strive to reveal  $\mathcal{G}_d$  through the optimal attack model  $\mathcal{F}_{att_{\Delta\mathcal{G}}}$ . Similarly,  $\mathcal{G}_d = (\mathcal{V}_{rec_{\mathcal{V}_d}}, \mathcal{E}_{\mathcal{N}_{\mathcal{V}_d}^1}, \mathcal{X}_{rec_{\mathcal{V}_d}}) \neq \Delta\mathcal{G}$ , where  $\mathcal{V}_d$  is the node deletion set. For black-box GU-FGRA, attackers exploit the posterior probabilities  $P = (p_1, p_2, \dots, p_{|\mathcal{Y}|})$  obtained before and after node removals to estimate the gradient difference  $\Delta\hat{\nabla}\mathcal{L}(\theta_{\Delta\mathcal{G}_v})$  or  $\Delta\hat{\nabla}\mathcal{L}(\theta_{\Delta\mathcal{G}})$ , and then adopt the identical procedure used in the white-box setting.

### 3. Attack Framework Design

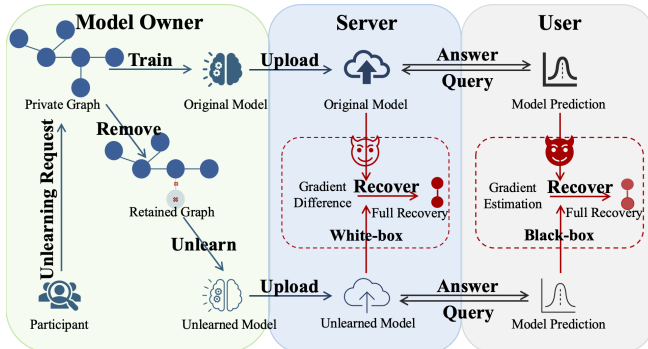


Figure 1: An overview of GraphToxin. The white-box GraphToxin uses gradient difference for full unlearned graph recovery. The black-box GraphToxin first estimates gradients and then exploits their difference for recovery.

#### 3.1. Threat Model

**3.1.1. Attacker’s Goal.** As mentioned above, attackers aim to fully reconstruct the unlearned graph—including the removed nodes, their affected nodes, their topological structures, and node features—rather than a simple combination of multiple feature recovery and neighboring link stealing attacks either for a single node or multiple node removals.

**3.1.2. Attacker’s Knowledge and Capabilities.** Graph unlearning generally involves three parties in practice: the model owner, the server and the users. The model owner trains a GNN on a private graph and then uploads it to the server. The server then deploys the model and packs it into an API for users to use, and the users can flexibly send queries to the server and receive prediction results [11], [18]. In compliance with legal regulations, upon receiving an unlearning request from a participant (i.e., a specific node in the training graph), the model owner must adopt graph unlearning methods to unlearn any information associated with that participant, and then upload the unlearned model

and delete the previous version. However, attackers can exploit the time gap between model updates to save a copy of the deleted model or perform model extraction attacks to steal it. Therefore, it is realistic to assume that attackers have access to both the original and unlearned models [11], [18]. We also assume attackers can master the number of changed nodes, edges, and corresponding labels. This is practical since such information can be obtained through simple count queries or by inspecting publicly released technical documents. These documents—which often detail data statistics and model information (e.g., node and edge size, label distribution, model name)—are common on MLaaS platforms to facilitate proper model use. Moreover, attackers can employ existing label inference techniques to recover labels, which serve as a cornerstone for subsequent reconstruction attacks [11], [19].

In contrast to existing graph reconstruction attacks, our threat model strictly assumes no access to partial node features, graph topology, or shadow datasets. This assumption is realistic, as private training graphs are proprietary and constitute valuable assets of companies and institutions, necessitating strong protections against potential attackers.

In reality, attackers can be an internal actor, such as honest-but-curious server administrators, they faithfully fulfill their responsibilities to serve users but are curious about the unlearned content upon new unlearning requests [11]. They normally deploy the unlearned model but secretly archive the old version. Alternatively, attackers can also be malicious external users, they can conduct model extraction attacks to obtain two copycats of the original and unlearned models. Even though these substitutes can leak much more information, we strictly assume that attackers only have access to the gradients of the original and unlearned models, without prior knowledge of the unlearning method or any partial information of the deleted content. Furthermore, auditors can act as a red team to launch GU-FGRA with only the minimal required knowledge in a data-free setting, enabling them to discover vulnerabilities and anomalies to improve the security and privacy of AI systems.

Under the black-box setting, we assume that attackers can only obtain the posterior probabilities of the original and unlearned GNNs. This more realistic assumption significantly increases the attack range in practice, as any attacker can impersonate as a normal user to query the models and exploit these posteriors to launch GU-FGRA.

#### 3.2. Attack Framework Design

We introduce GraphToxin, the first full graph reconstruction attack against graph unlearning. The framework

overview is shown in Figure 1. GraphToxin contains three modules: gradient matching, curvature matching and feature smoothness, detailed as follows.

**3.2.1. Gradient Matching.** Gradient matching is the foundational component of gradient inversion attacks tailored for federated learning. Given the model gradients for a single data point, gradient matching iteratively optimize the dummy input by minimizing the distance between its dummy gradients and the actual model gradients. The optimized dummy input finally ‘‘matches’’ the ground-truth data point. This matching degree is typically quantified using cosine similarity or L2 distance.

In the graph domain, gradient matching denotes the process of reducing the discrepancy between the dummy gradients of a dummy graph and the ground-truth model gradients, it can be formally defined as:

$$\tilde{\mathcal{G}} = \arg \min_{\tilde{\mathcal{G}}} D(\nabla \mathcal{L}(\mathcal{F}_\theta(\tilde{\mathcal{G}}), \mathcal{Y}), \nabla \mathcal{L}(\mathcal{F}_\theta(\mathcal{G}), \mathcal{Y})) \quad (2)$$

For simplicity, we denote  $\mathcal{L}(\mathcal{F}_\theta(\mathcal{G}), \mathcal{Y})$  as  $\mathcal{L}(\theta)$ , the gradients as  $\nabla \mathcal{L}(\theta)$  and the approximated gradients as  $\tilde{\nabla} \mathcal{L}(\theta)$ .

Since graph unlearning requires removing the deleted node  $v$ ’s influence, the difference between the gradients of the original model  $\nabla_{ori} \mathcal{L}(\theta)$  and the unlearned model  $\nabla_{un} \mathcal{L}(\theta^*)$  consequently encodes the unlearned information  $X_v$  and  $\mathcal{N}_v^1$ . Therefore, we exploit this difference  $\nabla_{ori} \mathcal{L}(\theta) - \nabla_{un} \mathcal{L}(\theta^*)$  ( $\Delta \mathcal{L}(\mathcal{G}_d, \theta, \theta^*)$  hereinafter) to recover the full unlearned graph  $\mathcal{G}_d$ , which can be represented as:

$$\tilde{\mathcal{G}}_d = \arg \min_{\tilde{\mathcal{G}}_d} D(\tilde{\Delta} \mathcal{L}(\tilde{\mathcal{G}}_d, \theta, \theta^*), \Delta \mathcal{L}(\mathcal{G}_d, \theta, \theta^*)) \quad (3)$$

For the choice of distance function  $D$ , existing gradient inversion attacks commonly use cosine similarity [11], [20] or L2 distance [21]. One empirical investigation [22] favors L2 distance for its superior attack performance while another [23] shows that cosine distance correlates more strongly with the reconstruction quality. Inspired by Fan et al. [24], we combine both metrics to leverage their complementary strengths. Specifically, we adopt Mean Squared Error (MSE), an L2-based metric, to measure the absolute distance in the high-dimensional gradient space while mitigating the magnitude influences of the huge number of gradients, and leverage cosine similarity for direction alignment. Following Fan et al. [24], we treat these two losses equally.

$$\begin{aligned} \mathfrak{L}_{grad} &= 1 - \frac{\langle \tilde{\Delta} \mathcal{L}(\tilde{\mathcal{G}}_d, \theta, \theta^*), \Delta \mathcal{L}(\mathcal{G}_d, \theta, \theta^*) \rangle}{\|\tilde{\Delta} \mathcal{L}(\tilde{\mathcal{G}}_d, \theta, \theta^*)\| \cdot \|\Delta \mathcal{L}(\mathcal{G}_d, \theta, \theta^*)\|} \\ &+ \frac{1}{M} \sum_{j=1}^M (\tilde{\Delta} \mathcal{L}(\tilde{\mathcal{G}}_d, \theta, \theta^*)_j - \Delta \mathcal{L}(\mathcal{G}_d, \theta, \theta^*)_j)^2 \end{aligned} \quad (4)$$

where  $M$  is the number of elements in the gradients.

However, gradient matching is necessary yet insufficient for recovery. The corresponding analysis is detailed below. **Necessity** Gradients manifest the learning behaviors of a trained model and encode high-dimensional, per-sample fingerprints of the training graph. Gradient matching exploits these fingerprints to recover the full graph by synthesiz-

ing a candidate graph and iteratively adjusting it until its generated gradients match the observed ones. This process effectively mimics the model’s learning behaviors and ‘‘back-propagates’’ information from the gradient space to the input space. Moreover, since gradients quantify how sensitive the model’s loss is to parameter changes, gradient matching inherently seeks to a candidate graph that elicits the same sensitivities in the trained model and implicitly prioritizes the features and structures that are most salient to the model’s learning process and ultimately contribute most to its decision boundary.

**Insufficiency** Gradient matching only provides coarse proxy signals, as multiple different candidate graphs can yield very similar gradients, hence, attackers may match gradients but still recover wrong node features or graph topology. This ambiguity stems from inherent GNN properties: since GNNs are permutation-invariant, isomorphic graphs can produce identical information flow and hence identical gradients. Moreover, complex graph topology and node features are entangled during GNN message passing, severely compromising the identifiability of individual graph components within a single gradient signal. These issues are particularly magnified in graph unlearning. First, attackers exploit the gradient difference between the original and unlearned GNNs for full graph recovery, which often has a much smaller magnitude than pure gradients and thus providing more ambiguous guidance for disentangling the attribution of each graph component. Second, graph unlearning methods can introduce noises through regularization or mixed optimization objectives, hereby corrupting the unlearning signal. Most importantly, GU-FGRA aims not only to recover  $X_v$  and  $\mathcal{N}_v^1$ , but also to reveal the node features  $X_{\mathcal{N}_v^1}$  of the affected nodes.  $\Delta \mathcal{L}(\mathcal{G}_d, \theta, \theta^*)$  can explicitly reflect  $X_v$  and  $\mathcal{N}_v^1$ , but not  $X_{\mathcal{N}_v^1}$ . The precise recovery of  $X_{\mathcal{N}_v^1}$  for a single node removal still poses extra challenges, not to mention the extension to multiple node removals.

**3.2.2. Curvature Matching.** Through the preceding analysis, we identify the key limitation in standard gradient matching: solely relying on the gradient difference matching before and after graph unlearning can be ambiguous. As depicted in the illustrative example in Figure 2, we simulate the unlearning effect (reflected in  $\mathcal{L}_2$ ) by adding noises and slightly changing the polynomial coefficients of a convex loss function  $\mathcal{L}_1$ . As shown in Figure 2.A, the gradients of  $\mathcal{L}_1$  and  $\mathcal{L}_2$  are almost identical and their small gradient difference is reflected in Figure 2.B. However, we identify two distinct points (marked in blue and pink) that produce identical gradient differences, yet exhibit the substantially different curvatures of the loss landscape as shown in Figure 2.C and D. To overcome this ambiguity and provide fine-grained signals for full unlearned graph recovery, we introduce a novel curvature matching module.

The subsequent theoretical proof of curvature matching is built upon the following two assumptions:

**Assumption 1 (Empirical Risk Function).** We assume that  $\mathcal{L}(\cdot)$  is twice continuously differentiable and the Hessian  $H = \nabla_{ori}^2 \mathcal{L}(\theta)$  is invertible and symmetric w.r.t. parameter

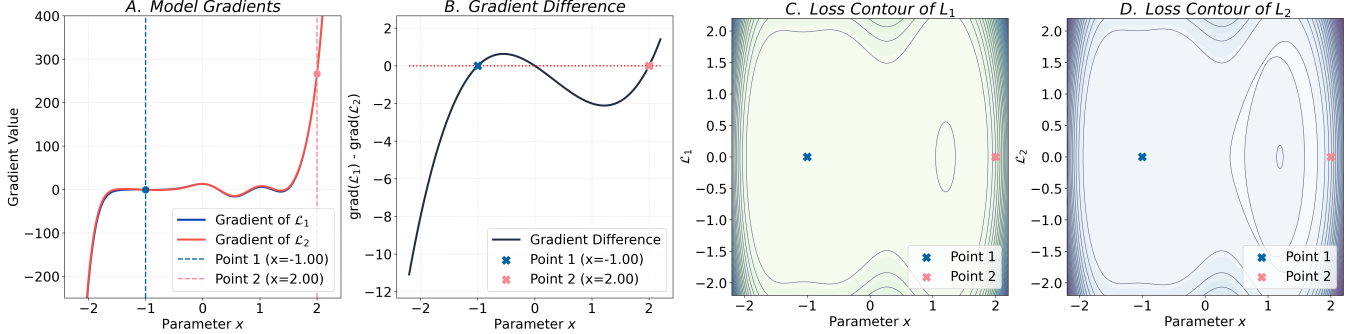


Figure 2: Illustrative Example of the Ambiguity of Gradient Difference Matching

θ. Following previous studies [25], [26], we add a damping term  $\lambda I$  to  $H$  if  $\mathcal{L}(\cdot)$  is non-convex.

**Assumption 2 (Small Parameter Change).** We assume that the parameter change  $\theta^* - \theta$  before and after graph unlearning is small.

We empirically find that this change is small (reflected in subsequent experiments). This finding aligns with theoretical works proving the change to be bounded [12], [27].

When the above assumptions hold, the first-order Taylor expansion of the gradient function  $\nabla \mathcal{L}(\cdot)$  around a stationary point  $\theta$  is:

$$\nabla_{un} \mathcal{L}(\theta^*) \approx \nabla_{ori} \mathcal{L}(\theta) + \nabla_{ori}^2 \mathcal{L}(\theta)(\theta^* - \theta) \quad (5)$$

GU-FGRA inherently generates a full recovered graph whose gradients can explain the parameter change [11]. Hence:

$$\Delta \tilde{\theta} \approx \theta^* - \theta \quad (6)$$

where  $\Delta \tilde{\theta}$  is the parameter induced by the dummy graph. Since the parameter  $\theta$  of the original model is fixed, w.l.o.g., for GU-FGRA, the attackers aim to find the parameter  $\tilde{\theta}$  so that  $\Delta \tilde{\theta} = \tilde{\theta} - \theta$ .

By combining Equation (5) and Equation (6), we state the following theorem:

**Theorem 1 (Fine-grained Curvature Matching).** When the above assumptions hold, matching the ground-truth gradient difference  $\Delta \mathcal{L}(\mathcal{G}_d, \theta, \theta^*)$  is equivalent to minimizing  $(\Delta_{syn} - \Delta_{obs})^T H^{-1}(\Delta_{syn} - \Delta_{obs})$ , where  $\Delta_{syn} = \Delta \mathcal{L}(\tilde{\mathcal{G}}_d, \theta, \theta^*)$ ,  $\Delta_{obs} = \Delta \mathcal{L}(\mathcal{G}_d, \theta, \theta^*)$ .

*Proof.* Based on Equation (5), we get  $\Delta_{obs} \approx H(\theta^* - \theta)$ . Since  $H$  is invertible,  $\theta^* - \theta \approx H^{-1} \Delta_{obs}$ . As for Equation (6), under the same linearized relation in Equation (5),  $\tilde{\theta} - \theta \approx H^{-1} \Delta_{syn}$ . Therefore, the attack goal is transformed to minimize the difference between  $H^{-1} \Delta_{obs}$  and  $H^{-1} \Delta_{syn}$ . Formally,  $H^{-1}(\Delta_{syn} - \Delta_{obs}) \approx 0$ . Take the  $H^{1/2}$  to the left-hand and right-hand side, then we get  $H^{-1/2}(\Delta_{syn} - \Delta_{obs}) \approx 0$ . Consider the squared L2 norm, the previous approximation equals to  $(\Delta_{syn} - \Delta_{obs})^T H^{-1}(\Delta_{syn} - \Delta_{obs})$ , hereby completing the proof.

However, utilizing  $H$  is computationally infeasible and expensive as it requires calculating and storing second-order derivatives. We leverage the Fisher Information Matrix  $F$  as

the surrogate. Specifically,  $F$  is defined as the covariance matrix of the gradient of the log-likelihood function with respect to the parameters  $\theta$ , quantifying the sensitivity of the model's predicted probability distribution to small changes in  $\theta$ . According to Rame et al. [28],  $F$  approximates  $H$  with probably bounded errors under regular conditions.

In practice, since the full  $F$  involves an expectation over all possible outputs, the empirical Fisher Information  $\tilde{F}$  is typically utilized as an efficient approximation [29]. Formally,  $\tilde{F}$  is denoted as:

$$\tilde{F} = \frac{1}{N_d} \sum_{i=1}^{N_d} (\nabla \log p(y_i | \tilde{\mathcal{G}}_d, \theta)) (\nabla \log p(y_i | \tilde{\mathcal{G}}_d, \theta))^T \quad (7)$$

where  $N_d = |\mathcal{V}_{recv_d}|$  is the node size of  $\mathcal{G}_d$ .

Replacing  $H$  with  $\tilde{F}$  in  $(\Delta_{syn} - \Delta_{obs})^T H^{-1}(\Delta_{syn} - \Delta_{obs})$ , we derive the following curvature matching loss:

$$\mathcal{L}_{curv} = (\Delta_{syn} - \Delta_{obs})^T \tilde{F}^{-1}(\Delta_{syn} - \Delta_{obs}) \quad (8)$$

The loss  $\mathcal{L}_{curv}$  naturally encodes the curvature of the loss landscape, providing much more precise guidance for full unlearned graph recovery. Not all gradient discrepancies between the synthetic and the full unlearned graphs are equally informative; some may stem from random noises while others are highly indicative of the ground-truth features and underlying graph structures. Introducing  $\mathcal{L}_{curv}$  can penalize the directions of high curvature, thereby biasing the optimization process toward plausible solutions with smooth landscapes and avoiding overfitting to noisy gradient directions. Moreover, the inclusion of  $F$  can capture the global features and structural dependencies and reflect how they are propagated during GNN message-passing and consequently projected into posterior probabilities. Compared to the simplex gradient matching, curvature matching encompasses a more holistic information flow, therefore yielding more realistic and accurate recovery.

**3.2.3. Feature Smoothness.** Most real-world graphs follow the homophily principle, where neighboring nodes tend to share similar features. Graph Dirichlet energy [3], [16], [30] explicitly encodes and quantifies this feature smoothness:

$$\mathcal{L}_{smooth} = \text{tr}(X^T L X) \quad (9)$$

where  $tr$  is the trace of a matrix,  $L = D - A$  is the laplacian matrix and  $D$  is the diagonal degree matrix.

This regularization penalizes sharp feature differences across connected nodes and suppresses degenerate and noisy solutions for realistic full graph recovery.

**3.2.4. Loss Function.** In summary, the final objective function of GraphToxin is as follows:

$$\mathcal{L}_{white} = \mathcal{L}_{grad} + \alpha_1 \mathcal{L}_{curv} + \alpha_2 \mathcal{L}_{smooth} \quad (10)$$

where the Fisher coefficient  $\alpha_1$  and the Laplacian coefficient  $\alpha_2$  control the fine-grained curvature matching and feature smoothness, respectively.

### 3.3. Extensions: Multiple Node Removal and Black-box GraphToxin

**3.3.1. Multiple Node Removal.** For multiple node removals, the topology of the full unlearned graph  $\mathcal{G}_d$  is no longer a simple star form. Instead, its topology  $\mathcal{E}_{\mathcal{N}_{\mathcal{V}_d^1}}$  becomes significantly more intricate due to the interconnection of removed nodes and their affected neighbors.

To simultaneously reconstruct node features and the more complex graph topology, we first initialize the graph topology by sampling a fixed number of edges using Bernoulli distribution [15]. This initialization is defined as  $A_0 \sim Bernoulli(p)$ , where  $p = \frac{|\mathcal{E}_{\mathcal{N}_{\mathcal{V}_d^1}}|}{|\mathcal{V}_{rec_{\mathcal{V}_d}}|}$  controls the expected edge density and statistically aligns with the known edge budget. Next, we adopt the same final objective function  $\mathcal{L}_{white}$  used for a single node removal, but we update the adjacency matrix  $A_\theta$  with the projected gradient method. Following Sinha et al. [15], each entry  $(i, j)$  of  $\tilde{A}$  is updated through the entry-wise projection operator as:

$$\hat{A}_{ij} = \text{proj}_{[0,1]}(\tilde{A}_{ij}) = \begin{cases} 1, & \tilde{A}_{ij} \geq 1 \\ 0, & \tilde{A}_{ij} \leq 0 \\ \tilde{A}_{ij}, & \text{otherwise} \end{cases} \quad (11)$$

Finally, we repeat the sampling process using the learned edge probabilities from the last iteration to generate the final reconstructed adjacency matrix  $\hat{A}$ .

**3.3.2. Black-box GraphToxin.** Distinct from the white-box setting, the black-box GraphToxin cannot access gradients and only relies on posterior probabilities. Notably, this most constrained attack remains feasible in reality. Inspired by Zhuang et al. [31], attackers first steal the original GNN  $\mathcal{F}_{ori}$  and unlearned GNN  $\mathcal{F}_{un}$  using a data-free and black-box model extraction attack, which involves a graph generator  $\phi_G(\cdot)$  and a surrogate model  $\phi_S(\cdot)$ . Specifically, attackers employ the zeroth-order gradient estimation [31], [32] to approximate the gradients of  $\mathcal{F}_{ori}$  and  $\mathcal{F}_{un}$ :

$$\tilde{\nabla} \mathcal{L}(\theta_{\phi_G(\cdot)}, \tilde{\mathcal{G}}, u_i) = \frac{d(\mathcal{L}(\theta_{\phi_G(\cdot)}, \tilde{\mathcal{G}} + u_i) - \mathcal{L}(\theta_{\phi_G(\cdot)}, \tilde{\mathcal{G}}))}{\epsilon} u_i \quad (12)$$

where the generated graph  $\tilde{\mathcal{G}} = \phi_G(\theta_{\phi_G}, z)$ ; the Gaussian noise  $u_i \sim N(0, I_D)$ , and  $\cdot$  can be  $\mathcal{F}_{ori}$  or  $\mathcal{F}_{un}$ , depending

on the stealing target.  $D$  is the feature dimension and  $\epsilon$  is a small positive constant called the smoothing factor. However, Equation (12) results in biased estimation as it only involves a single random direction. Following previous studies [31], [32], the average gradient estimation from  $m$  different random directions is required for precise gradient estimation, which is denoted as:

$$\tilde{\nabla} \mathcal{L}(\theta_{\phi_G(\cdot)}, \tilde{\mathcal{G}}) = \frac{1}{m} \sum_{i=1}^m \tilde{\nabla} \mathcal{L}(\theta_{\phi_G(\cdot)}, \tilde{\mathcal{G}}, u_i) \quad (13)$$

We adopt the same architecture and full parameterization trick as Zhuang et al. [31] to generate the query graph  $\tilde{\mathcal{G}}$ . To encourage the generator  $\phi_G(\cdot)$  producing more diverse and complex  $\tilde{\mathcal{G}}$ ,  $\phi_G(\cdot)$  is trained to maximize the disagreement between the posteriors of the victim and the surrogate models. Meanwhile, the surrogate model  $\phi_S(\cdot)$  is trained using the query responses of  $\tilde{\mathcal{G}}$  from the victim model. For details, we refer the interested readers to Zhuang et al. [31].

Once attackers obtain the copycats  $\tilde{\mathcal{F}}_{ori}$  and  $\tilde{\mathcal{F}}_{un}$ , they exploit the gradient difference between these copycats with the same  $\mathcal{L}_{white}$  for full unlearned graph recovery. However, the reconstruction quality highly depends on the stealing quality, and the gradient difference induced by two copycats inevitably introduces noises. To mitigate these issues, we add the following loss as the semantic calibration in  $\mathcal{L}_{white}$ :

$$\mathcal{L}_{seman} = CE(\tilde{\mathcal{G}}_d, Y_d) = - \sum_{i=1}^{|\mathcal{V}_{rec_{\mathcal{V}_d}}|} Y_{d_i} \cdot \log p_{d_i} \quad (14)$$

where  $CE$  is the cross-entropy loss to minimize the discrepancies between the ground-truth labels and the queried predictions of the recovered nodes in the synthetic graph  $\tilde{\mathcal{G}}_d$ .

Therefore, the final objective  $\mathcal{L}_{black}$  of the black-box GraphToxin is updated as:

$$\mathcal{L}_{black} = \mathcal{L}_{grad} + \alpha_1 \mathcal{L}_{curv} + \alpha_2 \mathcal{L}_{smooth} + \alpha_3 \mathcal{L}_{seman} \quad (15)$$

where  $\alpha_3$  is the calibration coefficient.

### 3.4. Evaluation Framework Design

To answer the third key research question, we propose a systematic and comprehensive evaluation framework for GraphToxin. We will further demonstrate its necessity along with the worst-case evaluation in Experimental Validation.

#### 3.4.1. Feature-level Evaluation.

**Root Normalized Mean Squared Error (RMSE)** Following Sinha et al. [15], we leverage RMSE to measure the discrepancies between the recovered node features and their corresponding ground-truth node features.

$$\text{RMSE}(X_v, \tilde{X}_v) = \frac{\|X_v - \tilde{X}_v\|}{\|X_v\|} \quad (16)$$

For each  $v \in \mathcal{V}_{rec_{\mathcal{V}_d}}$ , we compute its RMSE to the corresponding node features in the original training graph  $\mathcal{G}$  and then report the average RMSE of all nodes in  $\mathcal{V}_{rec_{\mathcal{V}_d}}$ .

### 3.4.2. Global-level Evaluation.

For a single node removal, the graph topology is fixed in GraphToxin. There is no need to introduce structural-level evaluation. While for multiple node removals, traditional metrics like Area Under Curve (AUC) or Average Precision (AP) focus only on the existence of individual links and fail to capture the holistic structural patterns. Instead, we provide the following global-level metrics to jointly evaluate the full feature and topology recovery.

**Embedding Distance (ED)** During message passing, node embedding inherently encodes node features, and local and high-level structural patterns. Consequently, quantifying the similarity between the node embeddings of the recovered and ground-truth deleted graphs provides a more holistic view compared to single-modality metrics. We consider the squared quadratic Wasserstein distance ( $p=2$ ) [33] to measure this similarity, denoted as  $W_2(\hat{H}^k, H^k)$ .

**Pyramid Match Graph Kernel (PMGK)** PMGK is a robust measure for graph matching [34]. It can capture structural similarities across multiple scales, from local motifs to global community structures. Specifically, we discretize the continuous embeddings of the recovered and ground-truth graphs into a set of discrete labels via K-means clustering, thus grouping nodes with similar structural or semantic patterns. Finally, we create a multi-resolution histogram of these labels of each graph and then take a weighted sum of the intersections of these two histograms. In our experiment, we utilize the grakel library [35] to compute PMGK.

**3.4.3. Performance-level Evaluation.** Intuitively, if two graphs are similar and fed into the same model, their outputs should also be similar. We adopt the following performance-level metrics to assess this alignment.

**Attack Accuracy (ATT. ACC)** Attack accuracy quantifies how effectively GraphToxin recovers the functionally equivalent full unlearned graph from graph unlearning.

**Attack Fidelity (ATT. FID)** Attack fidelity quantifies how accurately the recovered graph can yield the same model-specific predictions as the full ground-truth unlearned graph.

**Posterior Wasserstein Distance (PWD)** PWD measures how closely the recovered graph replicates the confidence and uncertainty of the ground-truth unlearned graph. Similarly, we adopt the squared quadratic Wasserstein distance ( $p=2$ ) to compare these two posterior probabilities.

## 4. Experimental Validation

In this section, we conduct empirical experiments on diverse GNN variants, graph unlearning methods and graph datasets to answer our three primary research questions. Specifically, we investigate the following key subquestions:

- SQ1:** Why is comprehensive evaluation necessary?
- SQ2:** How GraphToxin performs for a single node removal?
- SQ3:** Can GraphToxin flexibly adapt to different graph unlearning methods and GNN backbones?
- SQ4:** How GraphToxin performs in worst-case scenarios?
- SQ5:** Which impact factors dominate GraphToxin?
- SQ6:** How GraphToxin performs in multiple node removals?

**SQ7:** Can GraphToxin be extended to the black-box setting?

**SQ8:** How resilient is GraphToxin against defenses?

### 4.1. Setups

**4.1.1. Datasets.** To assess the effectiveness of GraphToxin, we conduct experiments on three publicly available graph datasets: Cora, PubMed [36], and Amazon-Photo (Photo) [37]. We provide the data details in Appendix A.1.

**4.1.2. Unlearning Methods.** We consider the following graph unlearning methods:

- 1) **Exact Unlearning:** After node removals, we directly retrain the GNNs from scratch (Retraining).
- 2) **Approximate Unlearning:** We consider two state-of-the-art graph unlearning methods with distinct frameworks: MEGU [13] and ETR [14]. MEGU is a learning-based method that employs predictive and unlearning modules to mitigate unlearning effects, while ETR is a training-free method designed to erase the influence of deleted nodes and rectify the collateral damage to their neighbors.

**4.1.3. GNN Variants.** We use three classical GNN backbones: GCN [38], GraphSAGE [39] and SGC [40].

**4.1.4. Baselines.** Since GraphToxin is the first graph reconstruction attack against graph unlearning, there is no reliable existing method to compare. Instead, we consider:

- 1) **Random Graph (Rand.):** We generate random graphs using Gaussian noises without parameter updates.
- 2) **Learning with A Few Epochs (FewE.):** We train GraphToxin for only the top 1% epochs.

**4.1.5. Implementation.** All experiments are implemented on 4 Nvidia A100 GPUs. For detailed hyperparameter settings and architecture choices, please refer to Appendix A.2.

### 4.2. Attack Performance (SQ1 - SQ3)

The original training and graph unlearning results with different GNN backbones across three graph datasets are detailed in Table 5 in Appendix A.3, which confirm the effectiveness and consistency of all considered graph unlearning methods. Specifically, all graph unlearning methods achieve very similar performance on three GNN backbones, with less than 1% variation. The GCN backbone is the best attack target (the highest performance) in Cora and PubMed while SGC excels in Photo, with less than 2% variation from GCN’s results. Among the unlearning methods, ETR achieves superior performance in Cora and PubMed, while Retraining performs better with GCN and SGC backbones, and MEGU exceeds others with GraphSAGE in Photo. For the removal settings, we observe that removing 10% of the highest-degree nodes (the worst-case scenario) results in larger performance degradation compared to the random node removal. This degradation is amplified for sparse and smaller-scale graphs, highlighting the necessity of a rigorous worst-case evaluation for graph unlearning.

**4.2.1. Necessity of Comprehensive Evaluation.** We first motivate the necessity for a comprehensive evaluation framework before presenting our detailed attack analysis. We contend that the standard NRMSE metric in existing graph recovery attacks [15] is insufficient on its own for assessing the reconstruction quality of node features. As shown in Table 2, even a randomly generated graph can achieve a deceptively low NRMSE while failing on crucial performance-level metrics such as attack accuracy, fidelity, and posterior Wasserstein distance. This obscurity highlights how NRMSE can conceal significant qualitative differences between a recovered graph and the ground-truth, which are further amplified by the message-passing paradigm and ultimately projected as a large semantic gap. Hence, more sensitive metrics are required to discern subtle variations. Specifically, when NRMSE values are nearly identical, embedding distance can reveal a significant divergence between graphs. Moreover, since a single node removal induces a fairly small gradient change, GraphToxin achieves consistent performance across various unlearning methods. Notably, all results are different, but some variations cannot be reflected on the scale of  $1e-2$ . However, PMGK can reflect such minimal changes that are imperceptible to other metrics.

**4.2.2. Effectiveness.** As shown in Table 2, GraphToxin consistently and significantly outperforms the two baselines across all experimental settings in nearly every reconstruction quality and performance-level evaluation metrics. The superiority of GraphToxin generalizes across distinct graph datasets and successfully targets various graph unlearning methods. Meanwhile, GraphToxin’s overall advantage holds under both random and worst-case node removal scenarios, highlighting its robustness. Notably, GraphToxin achieves up to **11.14 $\times$**  better performance than the random generation method on the performance-level metrics in Cora, and up to **86.73 $\times$**  better in Photo. However, averaging performance across recovered graphs from the random node removal can be misleading, motivating the need for a worst-case analysis. PubMed exemplifies this problem. Due to its high sparsity and small label space (with only three labels), even a randomly generated graph can yield deceptively strong results on the performance-level metrics, as the random node removal often results in simpler recovery targets. This effect can artificially inflate the average result, offsetting the random baseline’s weaker performance on more complex and larger-scale graphs. In contrast, a worst-case evaluation targeting the top 10% highest-degree nodes removes this masking effect, revealing a substantial decrease in the random graph’s performance and thus providing a more accurate assessment of GraphToxin’s efficacy.

**4.2.3. Flexibility.** To answer SQ3, we evaluate the performance of GraphToxin across different graph unlearning methods and GNN backbones.

**Graph Unlearning** From Table 2, GraphToxin demonstrates superior and consistent performance across all unlearning methods. Specifically, in Cora, the attack against Retraining achieves the highest NRMSE and attack accuracy in both random and worst cases. It also excels in embedding

distance, attack fidelity, and posterior Wasserstein distance (random case), and in PMGK and attack fidelity (worst case). The attack against MEGU outperforms others in embedding distance and posterior Wasserstein distance in the worst case, and in attack fidelity in the random case. In PubMed, GraphToxin produces very similar results in nearly all metrics, except for PMGK, where ETR stands out in the random case while Retraining leads in the worst case. In Photo, the attack against ETR performs better in NRMSE (both cases) and exceeds others in embedding distance and attack accuracy (worst case), and in PMGK (random case), while Retraining excels in PMGK, attack fidelity and posterior Wasserstein distance in the worst case. Despite these differences, the overall variations among unlearning methods are negligible, with only Retraining outperforming by a maximum of 2.5% in attack accuracy in Cora.

**GNN Backbones** Since GraphToxin achieves consistent performance across different graph unlearning methods on three graph datasets, in this experiment, we directly assess the worst unlearning case—Retraining—on different GNN backbones. As shown in Table 6 in Appendix A.4, similarly, GraphToxin retains its superiority and generalization across all GNN backbones and graph datasets. In Cora, GraphToxin with the GCN backbone outperforms GraphSAGE and SGC in all performance-level metrics. It leads in NRMSE and PMGK in the random case and embedding distance in the worst case. GraphSAGE achieves the best NRMSE in the worst case and embedding distance in the random case, while SGC excels in PMGK in the worst case. In PubMed, GraphToxin with the GCN backbone performs better in embedding distance, PMGK and posterior Wasserstein distance (worst case), and surpasses others in attack accuracy (random case). GraphSAGE exceeds in NRMSE and attack fidelity (worst case), and in PMGK (random case), while SGC excels in NRMSE, embedding distance, attack fidelity and posterior Wasserstein distance (random case), and in attack accuracy (worst case). In Photo, GraphToxin with the GCN backbone achieves superior NRMSE and embedding distance in the random case, and in PMGK in both cases. GraphSAGE exceeds in attack accuracy, fidelity, and posterior Wasserstein distance in the random case, while SGC excels in NRMSE embedding distance, attack accuracy, fidelity, and posterior Wasserstein distance in the worst case.

In conclusion, there is no universally most vulnerable GNN due to the complex interplay among model architecture, graph sparsity and homophily. We provide the following plausible explanations: 1) GCN aggregates information over local neighborhoods. This paradigm creates a strong and predictable link between a node’s features and its neighbors for full graph recovery. However, this “imprint” may fail due to rapid aggregation expansion and subsequent over-smoothing. Hence, GCN obtains more competitive performance in small-scale, sparse and homophilous graphs like Cora. 2) Since GraphSAGE utilizes neighbor sampling rather than the full neighborhood aggregation, gradients are influenced by only a subset of the true local structure in each forward pass. This inherent randomness can obfuscate GraphToxin as it relies on incomplete gradients as guidance,

TABLE 2: **The Performance of GraphToxin for A Single Node Removal (Backbone: GCN).** Unit: **1e-2**. Arrow indicates the direction of better performance and the **blue** color denotes the superb ‘**best**’ results (in **bold**).

Dataset	GU	Baseline	NRMSE( $\downarrow$ )		ED( $\downarrow$ )		PMGK( $\uparrow$ )		ATT. ACC( $\uparrow$ )		ATT. FID( $\uparrow$ )		PWD( $\downarrow$ )	
			Random	Worst	Random	Worst	Random	Worst	Random	Worst	Random	Worst	Random	Worst
Cora	Retrain	Rand.	6.59	3.61	78.76	72.45	84.35	68.35	6.79	9.18	6.31	7.48	82.79	80.23
		FewE	5.08	2.84	73.11	65.96	<b>84.62</b>	<b>68.79</b>	57.50	39.29	56.67	37.98	40.47	56.30
		Toxin	<b>4.11</b>	<b>1.95</b>	<b>71.38</b>	<b>52.35</b>	84.05	67.21	<b>72.21</b>	<b>84.72</b>	<b>69.00</b>	<b>77.97</b>	<b>29.66</b>	<b>22.35</b>
	MEGU	Rand.	6.59	3.61	78.76	72.45	84.19	<b>68.64</b>	6.79	9.18	6.31	7.48	82.79	80.23
		FewE	5.08	2.84	73.16	66.02	84.11	67.73	57.50	39.29	56.67	37.98	40.48	56.31
		Toxin	<b>4.23</b>	<b>2.10</b>	<b>71.84</b>	<b>51.18</b>	<b>84.30</b>	67.21	<b>71.14</b>	<b>82.22</b>	<b>70.31</b>	<b>77.85</b>	<b>30.22</b>	<b>20.72</b>
	ETR	Rand.	6.59	3.61	78.76	72.43	84.16	67.37	6.79	9.18	6.31	7.48	82.79	80.23
		FewE	5.08	2.84	73.16	66.02	<b>84.97</b>	<b>67.73</b>	57.50	39.29	56.67	37.98	40.48	56.31
		Toxin	<b>4.23</b>	<b>2.10</b>	<b>71.84</b>	<b>51.18</b>	84.14	66.92	<b>71.14</b>	<b>82.22</b>	<b>70.31</b>	<b>77.85</b>	<b>30.22</b>	<b>20.72</b>
PubMed	Retrain	Rand.	79.58	28.85	68.92	70.95	91.62	68.36	67.46	29.76	74.07	48.19	107.87	<b>2.59</b>
		FewE	77.73	27.99	<b>65.14</b>	<b>61.47</b>	<b>92.30</b>	<b>71.30</b>	67.46	77.19	74.08	67.20	<b>0.02</b>	10.61
		Toxin	<b>53.44</b>	<b>13.36</b>	74.17	63.16	90.66	70.68	<b>85.58</b>	<b>88.18</b>	<b>78.17</b>	<b>69.14</b>	18.65	12.24
	MEGU	Rand.	79.58	28.85	68.92	70.95	92.06	70.05	67.46	29.76	74.07	48.19	107.87	<b>2.59</b>
		FewE	77.73	27.99	<b>65.14</b>	<b>61.47</b>	<b>92.55</b>	<b>71.16</b>	67.46	77.19	74.07	67.20	<b>0.02</b>	10.61
		Toxin	<b>53.44</b>	<b>13.36</b>	74.17	63.16	91.17	70.42	<b>85.58</b>	<b>88.18</b>	<b>78.17</b>	<b>69.14</b>	<b>18.65</b>	<b>12.24</b>
	ETR	Rand.	79.58	28.85	68.92	70.95	91.59	69.17	67.46	29.76	74.07	48.19	107.87	<b>2.59</b>
		FewE	77.73	27.99	<b>65.14</b>	<b>61.47</b>	<b>92.61</b>	<b>72.63</b>	67.46	77.19	74.08	67.20	<b>0.02</b>	10.61
		Toxin	<b>53.44</b>	<b>13.36</b>	74.17	63.16	91.53	69.05	<b>85.58</b>	<b>88.18</b>	<b>78.17</b>	<b>69.14</b>	<b>18.65</b>	<b>12.24</b>
Photo	Retrain	Rand.	<b>0.61</b>	<b>0.31</b>	92.58	107.83	<b>69.33</b>	<b>63.29</b>	26.01	2.98	25.20	0.93	74.48	92.92
		FewE	<b>0.61</b>	<b>0.31</b>	51.46	68.21	68.03	58.10	67.44	28.76	68.02	28.74	28.12	62.26
		Toxin	0.64	0.34	<b>44.49</b>	<b>52.11</b>	66.33	49.65	<b>86.11</b>	<b>85.95</b>	<b>85.65</b>	<b>80.85</b>	<b>13.91</b>	<b>30.36</b>
	MEGU	Rand.	<b>0.61</b>	<b>0.31</b>	92.58	107.83	<b>68.42</b>	<b>63.22</b>	26.01	2.98	25.20	0.93	74.48	92.92
		FewE	<b>0.61</b>	<b>0.31</b>	51.46	68.21	68.08	57.81	67.44	28.76	68.02	28.74	28.12	62.26
		Toxin	0.64	0.34	<b>44.49</b>	<b>51.83</b>	66.36	49.06	<b>86.11</b>	<b>86.27</b>	<b>85.65</b>	<b>80.66</b>	<b>13.91</b>	<b>30.43</b>
	ETR	Rand.	<b>0.61</b>	<b>0.31</b>	92.58	107.83	<b>68.84</b>	<b>63.48</b>	26.01	2.98	25.20	0.93	74.48	92.92
		FewE	<b>0.61</b>	<b>0.31</b>	51.46	68.21	68.60	58.02	67.44	28.76	68.02	28.74	28.12	62.26
		Toxin	<b>0.61</b>	<b>0.31</b>	<b>44.49</b>	<b>51.83</b>	66.36	49.06	<b>86.11</b>	<b>86.27</b>	<b>85.65</b>	<b>80.66</b>	<b>13.91</b>	<b>30.43</b>

especially in the sparse graphs. However, in dense graphs like Photo, GraphToxin with the GraphSAGE backbone can still achieve promising attack results. 3) SGC employs linear multi-hop feature propagation. While its linearity offers a direct and simpler proxy for full graph recovery, its linear smoothing can also destroy fine-grained and node-specific details. This dual effect explains why SGC stands out in some metrics in PubMed and Photo while its performance degrades in Cora.

### 4.3. Parameter Studies (SQ4 and SQ5)

**4.3.1. Worst-case Analysis.** In previous subsections, we addressed the necessity and importance of the worst-case evaluation. Here we shift the focus to its analysis. As shown in Table 2 and Table 6, interestingly, in Cora, GraphToxin against all graph unlearning methods achieves better performance in the worst case in nearly all metrics, except for PMGK. Conversely, in PubMed and Photo, GraphToxin performs better in the random case in embedding distance, PMGK, attack fidelity and posterior Wasserstein distance. Additionally, GraphToxin with the GCN backbone also excels in attack accuracy in the random case.

For different GNN backbones, in Cora, GraphToxin in the random case achieves the best PMGK across all backbones. It also excels in embedding distance with SGC, and in attack accuracy, fidelity, and posterior Wasserstein distance with both GraphSAGE and SGC. In PubMed, it similarly leads in PMGK across all GNN backbones, and excels in embedding distance with SGC, in attack fidelity with GCN and SGC, and in posterior Wasserstein distance with SGC.

In Photo, GraphToxin in the random case surpasses others in PMGK and posterior Wasserstein distance across all backbones and obtains the best embedding distance, attack accuracy, and fidelity with both GCN and GraphSAGE.

In the worst-case scenario, the top 10% of nodes with the highest degrees are removed before GraphToxin attempts to reconstruct the full unlearned graph. Removing these highly influential structural hubs poses extra challenges, as the attack’s efficacy dependent on a delicate trade-off. While a moderate expansion of local neighborhoods can yield more informative gradients for graph recovery, these signals may also be distorted by over-smoothing or the loss of crucial semantic and structural details, particularly within heterogeneous neighborhoods or under linear smoothing effects.

**4.3.2. Deletion Graph Size.** Since we apply the same hyperparameter setting across all experiments to ensure a fair comparison, the reported results therefore represent a benchmark. We anticipate that case-specific hyperparameter tuning for each full recovered graph could yield further improvements in attack efficacy.

From Figure 5 in Appendix A.5, we consistently observe that the attack performance is highly volatile when the unlearned graph size is small, particularly for embedding distance, attack accuracy and fidelity, and posterior Wasserstein distance. As the size increases, the attack performance tends to stabilize and converge across different GNN backbones. Specifically, GraphToxin with the GCN backbone excels in the majority of settings. While GraphSAGE and SGC can diverge from GCN when the graph size ranges from 20–30 in Cora, their results ultimately converge as the graph size

increases. NRMSE remains relatively flat and low, indicating its insensitivity to the deletion graph size. PMGK generally exhibits a negative correlation with the graph size. However, excluding GCN in Photo, its PMGK rebounds when the graph size becomes substantially large.

**4.3.3. Node Homophily.** From Figure 6 in Appendix A.6, consistent attack performance is observed across diverse GNN backbones and graph datasets. Consistent with previous findings, GraphToxin with the GCN backbone achieves superior performance in nearly all metrics. However, GraphSAGE and SGC diverge from GCN in embedding distance, attack accuracy and fidelity, and posterior Wasserstein distance when node homophily approaches 1. Outside of this extreme range, the attack performance across all GNN backbones tends to converge. We speculate that perfect or near-perfect homophilous neighborhoods may lead to non-distinct node embeddings, resulting in uninformative gradients that hinder full graph recovery. NRMSE remains consistently flat and low, indicating its general insensitivity to node homophily. PMGK, however, exhibits a slight positive correlation. Unlike Cora and Photo, the PMGK curve shows distinct turning points, suggesting a more nuanced, non-linear dependency on node homophily.

**4.3.4. Fisher Coefficient.** The curvature matching module is a key component in GraphToxin, hence, we compare GraphToxin with and without this module to analyze its contribution for full graph recovery. We vary its Fisher coefficient from  $\{0, 0.01, 0.1, 1, 10\}$ . Setting the coefficient to 0 is equivalent to an ablation study of the module. From Figure 3, the results empirically prove the effectiveness of curvature matching, as performance in most metrics improves when the coefficient is non-zero. Consistent with previous findings, targeting the worst-case node removal generally yields more effective performance than the random removal. However, there are several notable exceptions. The random case significantly outperforms the worst case in PMGK across all coefficients. Additionally, the random case excels in attack fidelity for the fisher coefficient  $\alpha_1$  of 0.01 and 0.1, and in posterior Wasserstein distance when  $\alpha_1 \in \{0, 0.01, 0.1\}$ . Overall, GraphToxin achieves competitive performance when  $\alpha_1 \in \{0.01, 0.1, 1\}$  and yields the relatively optimal results for both random and worst cases when  $\alpha_1 = 0.1$ .

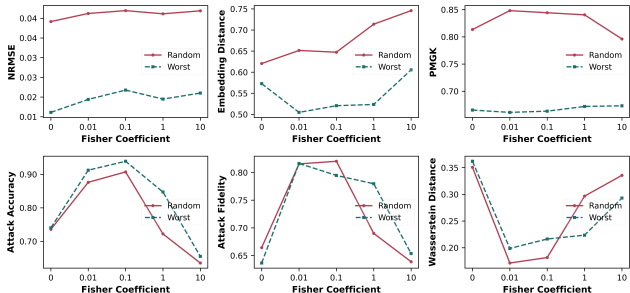


Figure 3: Impact of Fisher Coefficient

**4.3.5. Laplacian Coefficient.** We further assess the contribution of the feature smoothing module. Since prior studies set their Laplacian coefficients ( $\alpha_2$ ) to fairly small values [15], [16], we tune  $\alpha_2 \in \{0, 1e-7, 1e-5, 1e-3, 0.1\}$ . From Figure 4, the attack results demonstrate the effectiveness of this module. We also observe that targeting the worst-case node removal outperforms the random removal in nearly all metrics. The random case only surpasses the worst case in PMGK and attack accuracy, fidelity, and posterior Wasserstein distance when  $\alpha_2 = 0$ . Overall, GraphToxin achieves superior performance when  $\alpha_2 \in \{1e-7, 1e-5\}$ .

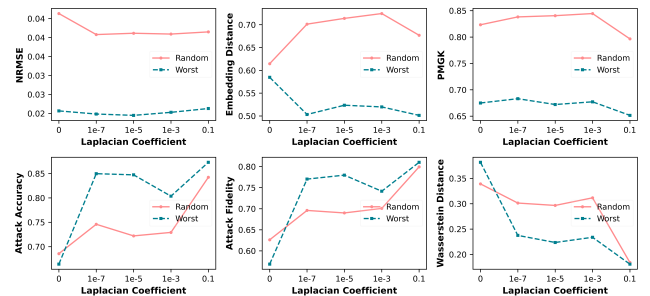


Figure 4: Impact of Laplacian Coefficient

#### 4.4. Extensions (SQ6 and SQ7)

Due to space limitations, we provide detailed performance and analysis of the extensions to multiple node removals and the black-box setting in Appendix A.7 and A.8, respectively.

#### 4.5. Discussion

**4.5.1. Defense (SQ8).** To investigate the performance of various defense mechanisms against GraphToxin, we utilize the most vulnerable and stable attack target—Retraining after a single node removal in the white-box setting. We adopt both in-processing and post-processing privacy-preserving techniques. Pre-processing techniques are out of our scope as they might cause obfuscation during node removals.

**Node-level Differential Privacy (Node-DP) in GNNs**  
 Node-DP in GNNs provides a formal privacy guarantee that protects an individual node and all its incident edges during message passing. Achieving this guarantee is substantially more difficult than enforcing standard DP or edge-level DP, as nodes introduce structural coupling and multi-hop dependencies that amplify per-sample sensitivity and complicate privacy accounting. Currently, there is no unified node-DP framework adapted to diverse GNN backbones. Existing studies either inject noises to shallow GNNs [41] or decouple graph convolutions through different architectures [42], [43]. Furthermore, a larger privacy budget is typically consumed for a better privacy and utility trade-off [44], [45], [46]. Consequently, realizing practical node-DP with competitive utility still remains an active research frontier.

Following Xiang et al. [46], we adopt HeterPoison to achieve node-DP. As their default privacy setting results

in unacceptable utility in our GNN backbones, we choose to tune the  $\sigma \in [0.006, 0.007, 0.008, 0.009, 0.01]$  in the symmetric multivariate Laplace noise  $\mathcal{LAP}(0, \sigma^2 \mathbb{I}^d)$ . This tuning yields the test accuracy of 79.40%, 76.00%, 69.90%, 61.00% and 51.90%, respectively. To balance utility and privacy, we select  $\sigma = 0.007$  to fight against GraphToxin.

From Table 3, even a rigorous privacy protection against GNNs cannot sufficiently defend GraphToxin. Under the node-DP guarantee, GraphToxin still retains competitive performance compared to the pure attack without any defense. Surprisingly, the attack performance even improves in attack accuracy. We speculate that this phenomenon occurs because DP noises can preferentially disrupt weak and unstable signals within the gradients, thus forcing GraphToxin to recover more robust graph components from more informative and stable gradients. While these components may not form a perfect replica of the original graph, they can contribute to the final node classification. In this sense, node-DP may act as a form of regularization, preventing GraphToxin from overfitting to trivial details.

**Gradient Compression (GC).** Given that GraphToxin exploits the real or estimated gradient difference for full graph recovery, it is imperative to enhance the privacy of released gradients. To this end, gradient compression techniques are widely employed against such gradient-based attacks [47]. Following Vogels et al. [48], we prune the smaller values to 0 by a  $p$  proportion to assess the impact of gradient sparsity on GraphToxin. We experiment with high pruning ratios of  $p \in [0.5, 0.7, 0.9]$ . The most stringent case,  $p = 0.9$ , enforces the extreme gradient sparsity where only very few gradients are preserved. The defense results are shown in Table 3. Similarly to node-DP, gradient compression cannot effectively defend GraphToxin. Interestingly, preserving only a fraction of the gradients can lead to comparable or even superior attack performance compared to using the full gradients as a proxy. When the pruning ratio increases, the overall attack performance slightly declines and then improves. Even in the most stringent scenario, GraphToxin under this privacy protection technique can exceed that of the undefended attack. This specific finding further reinforces our previous speculation: only retaining important and informative gradients rather than replicating trivial details can enhance the attack performance of GraphToxin.

#### 4.5.2. Limitation and Future Work.

**Assumption Relaxation** Similar to existing studies [11], [15], we assume that attackers can master node labels and the size of unlearned samples. Despite its feasibility, it is beneficial to propose a more advanced GU-FGRA without such information. A possible solution is to integrate label inference attacks into the GU-FGRA framework. When the size of the unlearned graphs is unknown, a Frobenious norm regularizer [15], [16] can be introduced to ensure graph sparsity. Furthermore, graph condensation-related metrics can be utilized to measure attack performance as the ground-truth deletion graph can be treated as an approximate condensed version of the recovered graph. We leave this investigation as future work.

**Large-scale Node Removal** This study mainly focuses on the effectiveness of GraphToxin in the context of small-scale multiple node removals. Although we explore the challenging worst-case scenario by simultaneously removing multiple highest-degree nodes, which results in a full deletion graph with a relatively large size, investigating the scalability of GraphToxin to large-scale multiple node removals presents a crucial direction for future work.

**More Worst-case Analysis** Since the degree of deleted nodes directly affects graph unlearning performance, we remove nodes with the highest degrees as the worst case in this study. Other metrics such as node influence [12], [49] can also be utilized for the worst-case analysis.

**Deep Investigation on Complex Interplays** We identify several interesting and counter-intuitive findings in this research. For instance, GraphToxin in the worst-case scenario achieves better overall attack performance than the random case. Furthermore, GraphToxin under a rigorous DP guarantee still retains competitive or even outstanding attack performance, and only preserving an extremely small fraction of the gradients can yield comparable or even superior attack performance compared to using the full gradients. An in-depth investigation should be conducted due to the complex interplays among model architectures, graph sparsity, node homophily and other possible factors.

## 5. Related Work

### 5.1. Graph Unlearning

According to Said et al. [4], existing graph unlearning methods can be categorized into exact graph unlearning and approximate graph unlearning.

**5.1.1. Exact Graph Unlearning.** GraphEraser pioneered the first graph unlearning framework [2]. Specifically, it partitions the original training graph into disjoint shards and then trains a separate GNN on each shard. Upon a new unlearning request, it directly deletes the node from the corresponding shard and subsequently retrains the shard GNN. Wang et al. [50] later adapted this framework into an inductive setting.

**5.1.2. Approximate Graph Unlearning.** GIF [12] utilizes the Graph Influence Function to estimate parameter changes after data removal and then computes a corrective update to these parameters to approximate the state of a model retrained on the reduced dataset. GNNDelete [51] optimizes two key objectives: deleted edge consistency, which scrubs the deleted influence from both model weights and neighboring representations, and neighborhood influence, which ensures that retained model knowledge is unaffected after deletion. MEGU [13] introduces a mutual evolution unlearning framework, which simultaneously optimizes a predictive module and an unlearning module to generate effective and reliable unlearning performance. ETR [14] proposes a two-stage training-free unlearning framework. In the Erase phase, ETR modifies model parameters to mitigate the impact of deleted samples and their propagated influence

TABLE 3: The Performance of Node-DP and Gradient Compression in Defending GraphToxin. Unit: **1e-2**. Arrow indicates the direction of better performance and the **bold** font denotes the ‘best’ results.

Defense	Type	NRMSE( $\downarrow$ )		ED( $\downarrow$ )		PMGK( $\uparrow$ )		ACC( $\uparrow$ )		FID( $\uparrow$ )		PWD( $\downarrow$ )	
		Random	Worst	Random	Worst	Random	Worst	Random	Worst	Random	Worst	Random	Worst
DP	Node	5.88	3.02	67.95	61.79	82.39	65.44	<b>86.72</b>	89.87	57.06	73.69	44.84	45.15
GC	p-0.5	4.15	<b>2.05</b>	70.40	48.40	<b>83.81</b>	67.20	76.62	<b>92.81</b>	68.64	79.26	31.21	<b>17.50</b>
	p-0.7	4.29	2.15	70.06	50.99	83.27	66.16	73.28	86.60	71.50	<b>80.54</b>	26.74	18.44
	p-0.9	<b>4.14</b>	2.15	<b>66.35</b>	<b>46.17</b>	82.53	<b>67.27</b>	<b>79.53</b>	90.31	<b>74.17</b>	79.60	<b>24.24</b>	17.79

on connected nodes. In the Rectify phase, it approximates the gradients of the remaining samples to enhance utility after graph unlearning.

## 5.2. Graph Reconstruction Attack against GNNs

The related work on graph reconstruction attacks against GNNs can be classified into the following four categories:

**5.2.1. Link Stealing Attack.** He et al. [5] introduced the first link stealing attack and provided a comprehensive attack taxonomy using various background knowledge. LinkTeller [6] exploits node features and labels to propose the first query-based link stealing attack via influence analysis in both transductive and inductive settings. LinkThief [52] combines node similarity, generalized structural features, and shadow graphs to assist link membership inference. Recently, TrendAttack [3] emerged as the first link stealing attack against graph unlearning to identify the link membership through confidence trend features. However, its attack assumptions are unrealistic in practice. Furthermore, it solely concentrates on an edge removal, whereas our research targets the hardest unlearning setting—node removal, posing substantially greater challenges and actual risks.

**5.2.2. Attribute Inference Attack against GNNs.** Duddu et al. [7] proposed the first attribute inference attack against GNNs. They exploited the node embeddings of partial nodes and their associated sensitive features to train a supervised attack classifier and ultimately infer the sensitive attributes of the target nodes. Olatunji et al. [8] developed three attribute inference attacks that leverage partial sensitive attributes, public non-sensitive attributes and shadow graphs to conduct multiple queries. However, these attacks solely target partial sensitive attributes, rather than full node feature recovery, which is one of the primary focuses of our work.

**5.2.3. Graph Topology Reconstruction Attack.** Duddu et al. [7] also designed the first graph topology reconstruction attack to exploit a strong correlation between publicly released embeddings and the ground-truth graph topology. Following the same attack setting, GraphMI [53] and Zhang et al. [9] reconstructed graph topology with similar graph statistics to the ground-truth through a graph encoder-decoder paradigm. Olatunji et al. [10] instead employed node features and their explanations for graph topology recovery. Specifically, they aimed to minimize the reconstruction error on node features and explanations and the

loss of node-level predictions. However, as previously mentioned, these attacks can only reconstruct graph topology instead of the full graph components. Furthermore, their attack assumptions are unrealistic, preventing generalization to the data-free black-box setting.

**5.2.4. Gradient Inversion Attack.** While the above three attack types have broad application scenarios, gradient inversion attacks (GIAs) against GNNs are specifically tailored for graph federated learning. GRAIN [17] presents the first GIA against GNNs for partial node feature and graph topology recovery. It employs the rank-deficiency of the GNN layers to reconstruct candidate subgraphs, iteratively filters unreliable ones, and finally combines these candidates with a depth-first search strategy for graph recovery. GLG [15] successfully validates that the subgraphs can be reconstructed through gradient matching in both node classification and graph classification tasks. However, these GIAs cannot be trivially adapted to graph unlearning.

## 6. Conclusion

In this study, we pioneer the investigation into the vulnerabilities of reconstructing the full unlearned graphs through graph unlearning. We propose GraphToxin, the first full graph reconstruction attack against graph unlearning. Specifically, we introduce a novel curvature matching module to provide fine-grained signals for full unlearned graph recovery in more realistic attack settings. We further extend GraphToxin to multiple node removals under both white-box and black-box settings. Furthermore, we present a rigorous and comprehensive evaluation framework, demonstrating the necessity of diverse evaluation metrics and worst-case analysis. Our attack results from extensive experiments confirm the effectiveness and flexibility of GraphToxin in both white-box and black-box settings for a single and multiple node removals. Notably, our assessment of existing defense mechanisms reveals their general ineffectiveness against this attack, highlighting the urgent need to develop more robust defensive countermeasures.

## Ethics Considerations

This study investigates vulnerabilities of graph unlearning solely on publicly available benchmark datasets and with unlearning algorithms tested on local devices. It does not directly compromise personal information or cause harm to real-world systems or servers. As a red team, we validate that the proposed attack reveals substantially more sensitive

information than existing inference attacks. The findings underscore the urgent need for robust countermeasures.

## LLM Usage Considerations

LLMs were used for editorial purposes in this manuscript, and all outputs were inspected by the authors to ensure accuracy and originality.

## References

- [1] K. Hjerppe, J. Ruohonen, and V. Leppanen, “The general data protection regulation: Requirements, architectures, and constraints,” in *2019 IEEE 27th International Requirements Engineering Conference (RE)*. IEEE, Sep. 2019. [Online]. Available: <http://dx.doi.org/10.1109/RE.2019.00036>
- [2] M. Chen, Z. Zhang, T. Wang, M. Backes, M. Humbert, and Y. Zhang, “Graph unlearning,” in *Proceedings of the 2022 ACM SIGSAC Conference on Computer and Communications Security*, ser. CCS ’22. New York, NY, USA: Association for Computing Machinery, 2022, p. 499–513. [Online]. Available: <https://doi.org/10.1145/3548606.3559352>
- [3] J. Zhang, Y. Wang, Z. Zhang, X. Liu, and S. Wang, “Unlearning inversion attacks for graph neural networks,” 2025. [Online]. Available: <https://arxiv.org/abs/2506.00808>
- [4] A. Said, Y. Zhao, T. Derr, M. Shabbir, W. Abbas, and X. Koutsoukos, “A survey of graph unlearning,” 2024. [Online]. Available: <https://arxiv.org/abs/2310.02164>
- [5] X. He, J. Jia, M. Backes, N. Z. Gong, and Y. Zhang, “Stealing links from graph neural networks,” in *30th USENIX Security Symposium (USENIX Security 21)*. USENIX Association, Aug. 2021, pp. 2669–2686. [Online]. Available: <https://www.usenix.org/conference/usenixsecurity21/presentation/he-xinlei>
- [6] F. Wu, Y. Long, C. Zhang, and B. Li, “Linkteller: Recovering private edges from graph neural networks via influence analysis,” in *2022 IEEE Symposium on Security and Privacy (SP)*, 2022, pp. 2005–2024.
- [7] V. Duddu, A. Boutet, and V. Shejwalkar, “Quantifying privacy leakage in graph embedding,” in *MobiQuitous 2020 - 17th EAI International Conference on Mobile and Ubiquitous Systems: Computing, Networking and Services*, ser. MobiQuitous ’20. New York, NY, USA: Association for Computing Machinery, 2021, p. 76–85. [Online]. Available: <https://doi.org/10.1145/3448891.3448939>
- [8] I. E. Olatunji, A. Hizber, O. Sihlovec, and M. Khosla, “Does black-box attribute inference attacks on graph neural networks constitute privacy risk?” 2023. [Online]. Available: <https://arxiv.org/abs/2306.00578>
- [9] Z. Zhang, M. Chen, M. Backes, Y. Shen, and Y. Zhang, “Inference attacks against graph neural networks,” in *31st USENIX Security Symposium (USENIX Security 22)*. Boston, MA: USENIX Association, Aug. 2022, pp. 4543–4560. [Online]. Available: <https://www.usenix.org/conference/usenixsecurity22/presentation/zhang-zhikun>
- [10] I. Olatunji, M. Rathee, T. Funke, and M. Khosla, “Private graph extraction via feature explanations,” *Proceedings on Privacy Enhancing Technologies*, vol. 2023, pp. 59–78, 04 2023.
- [11] H. Hu, S. Wang, T. Dong, and M. Xue, “Learn what you want to unlearn: Unlearning inversion attacks against machine unlearning,” in *2024 IEEE Symposium on Security and Privacy (SP)*, 2024, pp. 3257–3275.
- [12] J. Wu, Y. Yang, Y. Qian, Y. Sui, X. Wang, and X. He, “Gif: A general graph unlearning strategy via influence function,” in *Proceedings of the ACM Web Conference 2023*, ser. WWW ’23. New York, NY, USA: Association for Computing Machinery, 2023, p. 651–661. [Online]. Available: <https://doi.org/10.1145/3543507.3583521>
- [13] X. Li, Y. Zhao, Z. Wu, W. Zhang, R.-H. Li, and G. Wang, “Towards effective and general graph unlearning via mutual evolution,” *Proceedings of the AAAI Conference on Artificial Intelligence*, vol. 38, no. 12, pp. 13682–13690, Mar. 2024. [Online]. Available: <https://ojs.aaai.org/index.php/AAAI/article/view/29273>
- [14] Z.-R. Yang, J. Han, C.-D. Wang, and H. Liu, “Erase then rectify: a training-free parameter editing approach for cost-effective graph unlearning,” in *Proceedings of the Thirty-Ninth AAAI Conference on Artificial Intelligence and Thirty-Seventh Conference on Innovative Applications of Artificial Intelligence and Fifteenth Symposium on Educational Advances in Artificial Intelligence*, ser. AAAI’25/IAAI’25/EAAI’25. AAAI Press, 2025. [Online]. Available: <https://doi.org/10.1609/aaai.v39i12.33423>
- [15] D. A. Sinha, Y. Liu, R. Du, A. Markopoulou, and Y. Shen, “Gradient inversion attack on graph neural networks,” *Transactions on Machine Learning Research*, 2025. [Online]. Available: <https://openreview.net/forum?id=a0mLrqkWyx>
- [16] Z. Zhang, Q. Liu, Z. Huang, H. Wang, C.-K. Lee, and E. Chen, “Model inversion attacks against graph neural networks,” *IEEE Transactions on Knowledge and Data Engineering*, vol. 35, no. 9, pp. 8729–8741, 2023.
- [17] M. Drencheva, I. Petrov, M. Baader, D. I. Dimitrov, and M. Vechev, “GRAIN: Exact graph reconstruction from gradients,” in *The Thirteenth International Conference on Learning Representations*, 2025. [Online]. Available: <https://openreview.net/forum?id=7bAjVh3CG3>
- [18] M. Chen, Z. Zhang, T. Wang, M. Backes, M. Humbert, and Y. Zhang, “When machine unlearning jeopardizes privacy,” in *Proceedings of the 2021 ACM SIGSAC Conference on Computer and Communications Security*, ser. CCS ’21. New York, NY, USA: Association for Computing Machinery, 2021, p. 896–911. [Online]. Available: <https://doi.org/10.1145/3460120.3484756>
- [19] C. Fu, X. Zhang, S. Ji, J. Chen, J. Wu, S. Guo, J. Zhou, A. X. Liu, and T. Wang, “Label inference attacks against vertical federated learning,” in *31st USENIX Security Symposium (USENIX Security 22)*. Boston, MA: USENIX Association, Aug. 2022, pp. 1397–1414. [Online]. Available: <https://www.usenix.org/conference/usenixsecurity22/presentation/fu-chong>
- [20] J. Geiping, H. Bauermeister, H. Dröge, and M. Moeller, “Inverting gradients - how easy is it to break privacy in federated learning?” in *Proceedings of the 34th International Conference on Neural Information Processing Systems*, ser. NIPS ’20. Red Hook, NY, USA: Curran Associates Inc., 2020.
- [21] L. Zhu, Z. Liu, and S. Han, *Deep leakage from gradients*. Red Hook, NY, USA: Curran Associates Inc., 2019.
- [22] H. G. Hong, Y. Cho, H. Cho, J. Ahn, and J. Kim, “Foreseeing reconstruction quality of gradient inversion: an optimization perspective,” in *Proceedings of the Thirty-Eighth AAAI Conference on Artificial Intelligence and Thirty-Sixth Conference on Innovative Applications of Artificial Intelligence and Fourteenth Symposium on Educational Advances in Artificial Intelligence*, ser. AAAI’24/IAAI’24/EAAI’24. AAAI Press, 2024. [Online]. Available: <https://doi.org/10.1609/aaai.v38i11.29140>
- [23] C. Liu, J. Wang, , Y. Zhou, Y. Yuan, Q. Sheng, and K. Lu, “Afgi: Towards accurate and fast-convergent gradient inversion attack in federated learning,” 2024. [Online]. Available: <https://arxiv.org/abs/2403.08383>
- [24] M. Fan, F. Wang, C. Chen, and J. Zhou, “Boosting gradient leakage attacks: data reconstruction in realistic fl settings,” in *Proceedings of the 34th USENIX Conference on Security Symposium*, ser. SEC ’25. USA: USENIX Association, 2025.
- [25] H. Yuan, J. Xu, R. Huang, M. Song, C. Wang, and Y. Yang, “Can graph neural networks expose training data properties? an efficient risk assessment approach,” in *Advances in Neural Information Processing Systems*, A. Globerson, L. Mackey, D. Belgrave, A. Fan, U. Paquet, J. Tomczak, and C. Zhang, Eds.,

vol. 37. Curran Associates, Inc., 2024, pp. 69 361–69 385. [Online]. Available: [https://proceedings.neurips.cc/paper\\_files/paper/2024/file/806288e682d8a38c0bf21e37ab38af0a-Paper-Conference.pdf](https://proceedings.neurips.cc/paper_files/paper/2024/file/806288e682d8a38c0bf21e37ab38af0a-Paper-Conference.pdf)

[26] Z. Chen, P. Li, H. Liu, and P. Hong, “Characterizing the influence of graph elements,” in *The Eleventh International Conference on Learning Representations*, 2023. [Online]. Available: <https://openreview.net/forum?id=51GXyzOKOp>

[27] E. Chien, C. Pan, and O. Milenkovic, “Certified graph unlearning,” in *NeurIPS 2022 Workshop: New Frontiers in Graph Learning*, 2022. [Online]. Available: <https://openreview.net/forum?id=wCxIgc9ZCwi>

[28] A. Rame, C. Dancette, and M. Cord, “Fishr: Invariant gradient variances for out-of-distribution generalization,” in *Proceedings of the 39th International Conference on Machine Learning*, ser. Proceedings of Machine Learning Research, K. Chaudhuri, S. Jegelka, L. Song, C. Szepesvari, G. Niu, and S. Sabato, Eds., vol. 162. PMLR, 17–23 Jul 2022, pp. 18 347–18 377. [Online]. Available: <https://proceedings.mlr.press/v162/rame22a.html>

[29] R. Karakida, S. Akaho, and S.-i. Amari, “Universal statistics of fisher information in deep neural networks: Mean field approach,” in *Proceedings of the Twenty-Second International Conference on Artificial Intelligence and Statistics*, ser. Proceedings of Machine Learning Research, K. Chaudhuri and M. Sugiyama, Eds., vol. 89. PMLR, 16–18 Apr 2019, pp. 1032–1041. [Online]. Available: <https://proceedings.mlr.press/v89/karakida19a.html>

[30] V. Kalofolias, “How to learn a graph from smooth signals,” in *Proceedings of the 19th International Conference on Artificial Intelligence and Statistics*, ser. Proceedings of Machine Learning Research, A. Gretton and C. C. Robert, Eds., vol. 51. Cadiz, Spain: PMLR, 09–11 May 2016, pp. 920–929. [Online]. Available: <https://proceedings.mlr.press/v51/kalofolias16.html>

[31] Y. Zhuang, C. Shi, M. Zhang, J. Chen, L. Lyu, P. Zhou, and L. Sun, “Unveiling the secrets without data: Can graph neural networks be exploited through Data-Free model extraction attacks?” in *33rd USENIX Security Symposium (USENIX Security 24)*. Philadelphia, PA: USENIX Association, Aug. 2024, pp. 5251–5268. [Online]. Available: <https://www.usenix.org/conference/usenixsecurity24/presentation/zhuang>

[32] S. Kariyappa, A. Prakash, and M. K. Qureshi, “Maze: Data-free model stealing attack using zeroth-order gradient estimation,” in *Proceedings of the IEEE/CVF Conference on Computer Vision and Pattern Recognition (CVPR)*, June 2021, pp. 13 814–13 823.

[33] L. N. Vaserstein, “Markov processes over denumerable products of spaces, describing large systems of automata,” *Problemy Peredachi Informatsii*, vol. 5, no. 3, pp. 64–72, 1969.

[34] G. Nikolentzos, P. Meladianos, and M. Vazirgiannis, “Matching node embeddings for graph similarity,” *Proceedings of the AAAI Conference on Artificial Intelligence*, vol. 31, no. 1, Feb. 2017. [Online]. Available: <https://ojs.aaai.org/index.php/AAAI/article/view/10839>

[35] G. Siglidis, G. Nikolentzos, S. Limnios, C. Giatsidis, K. Skianis, and M. Vazirgiannis, “Grakel: A graph kernel library in python,” *Journal of Machine Learning Research*, vol. 21, no. 54, pp. 1–5, 2020. [Online]. Available: <http://jmlr.org/papers/v21/18-370.html>

[36] Z. Yang, W. Cohen, and R. Salakhudinov, “Revisiting semi-supervised learning with graph embeddings,” in *Proceedings of The 33rd International Conference on Machine Learning*, ser. Proceedings of Machine Learning Research, M. F. Balcan and K. Q. Weinberger, Eds., vol. 48. New York, New York, USA: PMLR, 20–22 Jun 2016, pp. 40–48. [Online]. Available: <https://proceedings.mlr.press/v48/yang16.html>

[37] O. Shchur, M. Mumme, A. Bojchevski, and S. Günnemann, “Pitfalls of graph neural network evaluation,” *ArXiv*, vol. abs/1811.05868, 2018. [Online]. Available: <https://api.semanticscholar.org/CorpusID:53303554>

[38] T. N. Kipf and M. Welling, “Semi-supervised classification with graph convolutional networks,” in *International Conference on Learning Representations*, 2017. [Online]. Available: <https://openreview.net/forum?id=SUJ4ayYg1>

[39] W. L. Hamilton, R. Ying, and J. Leskovec, “Inductive representation learning on large graphs,” in *Proceedings of the 31st International Conference on Neural Information Processing Systems*, ser. NIPS’17. Red Hook, NY, USA: Curran Associates Inc., 2017, p. 1025–1035.

[40] F. Wu, A. Souza, T. Zhang, C. Fifty, T. Yu, and K. Weinberger, “Simplifying graph convolutional networks,” in *Proceedings of the 36th International Conference on Machine Learning*. PMLR, 2019, pp. 6861–6871.

[41] A. Daigavane, G. Madan, A. Sinha, A. G. Thakurta, G. Aggarwal, and P. Jain, “Node-level differentially private graph neural networks,” 2022. [Online]. Available: <https://arxiv.org/abs/2111.15521>

[42] S. Sajadmanesh, A. S. Shamsabadi, A. Bellet, and D. Gatica-Perez, “Gap: Differentially private graph neural networks with aggregation perturbation,” in *32nd USENIX Security Symposium (USENIX Security 23)*. Anaheim, CA: USENIX Association, Aug. 2023.

[43] Q. Zhang, H. k. Lee, J. Ma, J. Lou, C. Yang, and L. Xiong, “Dpar: Decoupled graph neural networks with node-level differential privacy,” in *Proceedings of the ACM Web Conference 2024*, ser. WWW ’24. New York, NY, USA: Association for Computing Machinery, 2024, p. 1170–1181. [Online]. Available: <https://doi.org/10.1145/3589334.3645531>

[44] Y. Sun and M. Song, “Differentially private graph convolutional networks with privacy amplification,” in *2024 IEEE 23rd International Conference on Trust, Security and Privacy in Computing and Communications (TrustCom)*, 2024, pp. 2327–2335.

[45] D. Lei, Z. Song, Y. Yuan, C. Li, and L. Zhu, “Achieving personalized privacy-preserving graph neural network via topology awareness,” in *Proceedings of the ACM on Web Conference 2025*, ser. WWW ’25. New York, NY, USA: Association for Computing Machinery, 2025, p. 3552–3560. [Online]. Available: <https://doi.org/10.1145/3696410.3714555>

[46] Z. Xiang, T. Wang, and D. Wang, “Preserving node-level privacy in graph neural networks,” in *2024 IEEE Symposium on Security and Privacy (SP)*, 2024, pp. 4714–4732.

[47] R. Zhang, S. Guo, J. Wang, X. Xie, and D. Tao, “A survey on gradient inversion: Attacks, defenses and future directions,” in *Proceedings of the Thirty-First International Joint Conference on Artificial Intelligence, IJCAI-22*, L. D. Raedt, Ed. International Joint Conferences on Artificial Intelligence Organization, 7 2022, pp. 5678–5685, survey Track. [Online]. Available: <https://doi.org/10.24963/ijcai.2022/791>

[48] T. Vogels, S. P. Karimireddy, and M. Jaggi, *PowerSGD: practical low-rank gradient compression for distributed optimization*. Red Hook, NY, USA: Curran Associates Inc., 2019.

[49] W. Li, Z. Xiao, X. Luo, and Y. Sun, “Fast inference of removal-based node influence,” in *Proceedings of the ACM Web Conference 2024*, ser. WWW ’24. New York, NY, USA: Association for Computing Machinery, 2024, p. 422–433. [Online]. Available: <https://doi.org/10.1145/3589334.3645389>

[50] C.-L. Wang, M. Huai, and D. Wang, “Inductive graph unlearning,” in *Proceedings of the 32nd USENIX Conference on Security Symposium*, ser. SEC ’23. USA: USENIX Association, 2023.

[51] Y. Qin, Z. Zhang, X. Wang, Z. Zhang, and W. Zhu, “Nas-bench-graph: Benchmarking graph neural architecture search,” in *Advances in Neural Information Processing Systems*, S. Koyejo, S. Mohamed, A. Agarwal, D. Belgrave, K. Cho, and A. Oh, Eds., vol. 35. Curran Associates, Inc., 2022, pp. 54–69. [Online]. Available: [https://proceedings.neurips.cc/paper\\_files/paper/2022/file/004bed4e186fdd7ebb73aad6e97c2332-Paper-Datasets\\_and\\_Benchmarks.pdf](https://proceedings.neurips.cc/paper_files/paper/2022/file/004bed4e186fdd7ebb73aad6e97c2332-Paper-Datasets_and_Benchmarks.pdf)

[52] Y. Zhang, S. Meng, C. Chen, M. Peng, H. Gu, and X. Huang, “Linkthief: Combining generalized structure knowledge with node similarity for link stealing attack against gnn,” in *Proceedings of the 32nd ACM International Conference on Multimedia*, ser. MM ’24. New York, NY, USA: Association for Computing Machinery, 2024, p. 4947–4956. [Online]. Available: <https://doi.org/10.1145/3664647.3681381>

[53] Z. Zhang, Q. Liu, Z. Huang, H. Wang, C. Lu, C. Liu, and E. Chen, “Graphmi: Extracting private graph data from graph neural networks,” in *Proceedings of the Thirtieth International Joint Conference on Artificial Intelligence, IJCAI-21*, Z.-H. Zhou, Ed. International Joint Conferences on Artificial Intelligence Organization, 8 2021, pp. 3749–3755, main Track. [Online]. Available: <https://doi.org/10.24963/ijcai.2021/516>

[54] O. Shchur, M. Mumme, A. Bojchevski, and S. Günnemann, “Pitfalls of graph neural network evaluation,” 2019. [Online]. Available: <https://arxiv.org/abs/1811.05868>

[55] I. Loshchilov and F. Hutter, “Decoupled weight decay regularization,” in *International Conference on Learning Representations*, 2019. [Online]. Available: <https://openreview.net/forum?id=Bkg6RiCqY7>

## Appendix

### 1. Experimental Validation

**1.1. Datasets.** Cora and PubMed are small-scale and medium-scale citation networks with low average node degrees, where nodes represent scientific/medical publications, edges denote citations, and node features carry author’s personal information. Photo is a dense co-purchase graph, where nodes represent products, edges indicate frequent co-purchases, and features encode product reviews. The dataset statistics are shown in Table 4. We follow the classical data split setting in GNN benchmarking [51], [54] to randomly choose 20 nodes per class as the training set, 30 nodes per class as the validation set, and the rest as the test set.

TABLE 4: Detailed Graph Statistics

Datasets	Nodes	Edges	Features	Labels	Avg. Deg.	Homo. (%)
Cora	2,708	10,556	1,433	7	3.90	82.52
PubMed	19,717	88,648	500	3	4.50	79.24
Photo	7,650	238,162	745	8	31.13	83.65

### 1.2. Implementation.

- 1) **Victim GNN:** We consider 2-layer GNNs with the hidden dimension of 256 and a linear classifier for node classification tasks. We tune the learning rate from  $\{0.001, 0.005\}$ , and set the weight decay as  $5e-4$  and training epochs as 200.
- 2) **Graph Unlearning:** For MEGU, we adopt the default setting to set the unlearning rate as 0.05, weight decay as  $1e-4$ , tuning epoch as 100, and coefficients in the propagation process as 0.8, 0.5 and the coefficient in the loss function as 0.01. For ETR, we follow their default setting to tune the parameter-rectifying coefficient  $\lambda$  from  $\{0.001, 0.01, 0.3\}$ .
- 3) **GraphToxin:** For a single node removal, we select 10% random nodes or the top 10% nodes with the highest degrees from the training graph as attack targets, and report the average results throughout our paper. Please note that attackers do not know the exact location of

these nodes. They can only obtain the gradient difference between the original and unlearned GNNs. We set the Fisher coefficient as 1, the Laplacian coefficient as  $1e-5$ , and use AdamW [55] as the optimizer. Since multiple restarts to the optimizer (e.g, L-BFGS) from different starting points can significantly improve the reconstruction quality, for a fair comparison, we strictly follow the strategy in Sinha et.al. [15] for all experiments and only report the attack results with a single run of the optimizer. Similarly, we strictly set the attack learning rate as 0.01 for all experiments. Notably, better attack results can be achieved by carefully tuning this hyperparameter. The optimization runs for up to 10,000 iterations, but most attacks stopped earlier. Following Geiping et.al. [20] and Hu et.al. [11], we apply a step size decay after 3/8, 5/8, 7/8 of total iterations, using the multiplicative factor of 0.5.

### 1.3. Original and Unlearning Performance. See Table 5.

TABLE 5: The Performance of the Original and Unlearned GNNs for A Single Node Removal

Dataset	GNN	Original			Retraining			MEGU			ETR				
		ACC	AUC	Random	ACC	AUC	Worst	Random	ACC	AUC	Random	ACC	AUC	Worst	
Cora	GCN	80.20	<b>96.70</b>	80.05	<b>96.68</b>	79.99	<b>96.67</b>	80.06	<b>96.66</b>	80.52	<b>96.69</b>	80.57	<b>96.76</b>	80.69	<b>96.77</b>
	SAGE	<b>81.10</b>	96.61	<b>80.99</b>	96.66	<b>80.77</b>	96.64	80.04	96.54	79.94	96.52	80.80	96.56	80.86	96.57
	SGC	<b>81.10</b>	96.12	80.42	96.24	80.24	96.19	<b>80.64</b>	96.06	80.49	96.06	<b>81.10</b>	96.15	<b>81.10</b>	96.17
PubMed	GCN	77.40	<b>90.44</b>	77.78	<b>90.53</b>	<b>77.93</b>	<b>90.40</b>	<b>77.12</b>	<b>90.28</b>	<b>76.68</b>	<b>90.32</b>	77.53	<b>90.45</b>	77.75	<b>90.46</b>
	SAGE	76.90	89.44	75.53	89.23	74.80	89.08	76.22	89.51	76.05	89.50	76.68	89.54	76.48	89.53
	SGC	<b>78.20</b>	90.37	<b>77.92</b>	90.44	77.78	90.29	75.25	89.65	75.72	90.03	<b>78.05</b>	90.15	<b>78.12</b>	89.95
Photo	GCN	90.07	99.06	91.09	<b>99.05</b>	91.03	99.06	89.11	98.90	89.47	98.96	88.19	98.71	88.26	98.73
	SAGE	91.31	<b>99.28</b>	89.22	<b>99.05</b>	89.86	<b>99.09</b>	90.40	<b>99.14</b>	90.15	<b>99.14</b>	80.45	93.14	80.88	93.13
	SGC	<b>92.04</b>	99.02	<b>91.14</b>	98.99	<b>91.40</b>	99.00	<b>91.08</b>	98.88	90.97	98.94	<b>90.11</b>	99.03	<b>90.12</b>	<b>99.03</b>

### 1.4. Attack with GNN Backbones. See Table 6.

### 1.5. Impact Factor - Deletion Graph Size. See Figure 5.

### 1.6. Impact Factor - Node Homophily. See Figure 6.

**1.7. Multiple Node Removal.** We examine the efficacy of GraphToxin when removing 5, 10, 15 nodes simultaneously from the training graph, representing a more challenging unlearning scenario. For a fair comparison, all hyperparameters are kept identical to the single-node removal experiments. We consider two unlearning settings: in the random case, we randomly choose 5 disjoint sets for each removal size. While in the worst case, we select the top 25, 50, 75 nodes with the highest degrees and then partition them into 5 non-overlapping pairs based on their degree ranking. The average results are reported in Table 7. Notably, more competitive performance can be achieved by thorough parameter tuning.

Interestingly, the unlearning performance of Retraining in the worst-case multiple removal setting improves in accuracy but slightly decreases in AUC when more nodes are unlearned. As for attack performance, similarly as before, GraphToxin retains its superiority across all metrics in multiple node removals. When the number of deleted nodes increases, the attack performance on the reconstruction-related metrics improves, this is reflected in a reduction in NRMSE (all cases) and embedding distance (random case), and an increase in PMGK (worst case). In contrast, the trends for the performance-level metrics diverge in these two scenarios. For the worst-case removal, the attack’s

TABLE 6: **GraphToxin for A Single Node Removal with Different GNN Backbones (GU: Retraining).** Unit: **1e-2**. Arrow indicates the direction of better performance and the **blue** color denotes the superb ‘**best**’ results (in **bold**).

Dataset	GNN	Baseline	NRMSE(↓)		ED(↓)		PMGK(↑)		ATT. ACC(↑)		ATT. FID(↑)		PWD(↓)	
			Random	Worst										
Cora	GCN	Rand.	6.59	3.61	78.76	72.45	84.35	68.35	6.79	9.18	6.31	7.48	82.79	80.23
		FewE	5.08	2.84	73.11	65.96	<b>84.62</b>	<b>68.79</b>	57.50	39.29	56.67	37.98	40.47	56.30
		Toxin	<b>4.11</b>	<b>1.95</b>	<b>71.38</b>	<b>52.35</b>	84.05	67.21	<b>72.21</b>	<b>84.72</b>	<b>69.00</b>	<b>77.97</b>	<b>29.66</b>	<b>22.35</b>
	SAGE	Rand.	6.59	3.61	65.84	63.10	81.13	66.78	6.79	9.18	5.60	6.66	89.97	91.17
		FewE	6.01	3.24	67.71	64.14	80.10	66.94	38.69	28.63	33.93	24.36	56.19	65.42
		Toxin	<b>4.49</b>	<b>1.86</b>	<b>60.20</b>	<b>57.46</b>	<b>82.02</b>	<b>67.10</b>	<b>68.21</b>	<b>64.36</b>	<b>62.26</b>	<b>55.17</b>	<b>33.93</b>	<b>38.72</b>
	SGC	Rand.	6.59	3.61	95.25	91.71	81.41	67.04	6.79	9.18	8.10	9.26	84.98	80.48
		FewE	6.02	3.38	79.64	80.47	80.32	67.60	32.14	28.66	32.86	28.76	63.28	68.44
		Toxin	<b>4.35</b>	<b>2.16</b>	<b>65.47</b>	<b>66.94</b>	<b>84.04</b>	<b>67.56</b>	<b>72.50</b>	<b>61.03</b>	<b>67.50</b>	<b>55.99</b>	<b>30.97</b>	<b>41.89</b>
PubMed	GCN	Rand.	79.58	28.85	68.92	70.95	91.62	68.36	67.46	29.76	74.07	48.19	107.87	<b>2.59</b>
		FewE	77.73	27.99	<b>65.14</b>	<b>61.47</b>	<b>92.30</b>	<b>71.30</b>	67.46	77.19	74.08	67.20	<b>0.02</b>	10.61
		Toxin	<b>53.44</b>	<b>13.36</b>	74.17	63.16	90.66	70.68	<b>85.58</b>	<b>88.18</b>	<b>78.17</b>	<b>69.14</b>	18.65	12.24
	SAGE	Rand.	79.58	28.85	125.38	99.69	91.28	<b>72.51</b>	16.80	27.29	1.85	33.33	59.51	50.23
		FewE	79.12	28.03	86.45	<b>74.73</b>	<b>93.24</b>	69.55	65.21	64.13	55.82	64.16	25.55	32.54
		Toxin	<b>56.36</b>	<b>8.64</b>	<b>80.12</b>	76.06	91.32	60.54	<b>75.93</b>	<b>84.17</b>	<b>66.53</b>	<b>73.65</b>	<b>26.97</b>	<b>21.28</b>
	SGC	Rand.	79.58	28.85	81.82	83.96	91.55	69.86	67.46	29.76	73.15	46.39	<b>0.00</b>	<b>2.90</b>
		FewE	78.89	28.79	67.72	88.19	<b>91.99</b>	<b>69.92</b>	63.10	70.08	58.33	53.30	22.43	19.82
		Toxin	<b>42.97</b>	<b>14.55</b>	<b>64.16</b>	<b>70.67</b>	88.98	68.42	<b>81.88</b>	<b>92.48</b>	<b>81.88</b>	<b>69.40</b>	2.01	12.28
Photo	GCN	Rand.	<b>0.61</b>	<b>0.31</b>	92.58	107.83	<b>69.33</b>	<b>63.29</b>	26.01	2.98	25.20	0.93	74.48	92.92
		FewE	<b>0.61</b>	<b>0.31</b>	51.46	68.21	68.03	58.10	67.44	28.76	68.02	28.74	28.12	62.26
		Toxin	0.64	0.34	<b>44.49</b>	<b>52.11</b>	66.33	49.65	<b>86.11</b>	<b>85.95</b>	<b>85.65</b>	<b>80.85</b>	<b>13.91</b>	<b>30.36</b>
	SAGE	Rand.	<b>0.61</b>	<b>0.31</b>	116.19	127.18	<b>70.49</b>	<b>65.60</b>	26.01	2.98	26.56	3.89	74.77	95.12
		FewE	0.62	0.33	72.00	100.15	65.23	56.95	65.29	29.26	66.60	29.32	29.88	64.59
		Toxin	0.65	0.34	<b>55.44</b>	<b>70.72</b>	62.42	48.22	<b>94.52</b>	<b>87.79</b>	<b>91.74</b>	<b>81.67</b>	<b>11.51</b>	<b>30.41</b>
	SGC	Rand.	<b>0.61</b>	<b>0.31</b>	94.57	111.16	<b>71.23</b>	<b>63.74</b>	26.01	2.98	25.20	1.25	74.11	92.11
		FewE	<b>0.61</b>	<b>0.31</b>	58.26	56.17	68.42	60.97	64.69	45.54	65.99	47.94	26.50	41.42
		Toxin	0.66	0.33	<b>56.02</b>	<b>47.60</b>	65.29	45.59	<b>80.78</b>	<b>90.39</b>	<b>76.55</b>	<b>85.76</b>	<b>21.05</b>	<b>26.89</b>

performance steadily degrades as more nodes are removed. The random case, however, exhibits a non-monotonic trend, where the performance first improves and then declines. Though targeting multiple node removals results in a decrease in overall attack performance compared to the single-node scenario, GraphToxin remains a potent threat.

**1.8. Black-box Setting.** We also assess the performance of GraphToxin under the most intractable black-box setting. Inspired by Zhuang et al. [31], we utilize a GCN with 2 layers and 256 hidden units as a copycat, and a 3-layer MLP with 128 and 256 hidden units as a full-parameter graph generator. We set the query graph size as 250 with 32 feature dimensions. During model stealing, each query involves training the generator 2 times with a learning rate of  $1e-6$  and training the copycat 5 times with a learning rate of 0.001. The total number of queries is set to 100. The stealing performance of the original GNN is 79.40% in accuracy and 96.12% in AUC while the stealing performance of Retraining for both a single and multiple node removals improves in accuracy and slightly declines in AUC. For GraphToxin, we use the exactly same hyperparameter settings as before. As for the newly added semantic calibration module, we set its coefficient as 50 for the single node removal and 5000 for the multiple node removal, as the latter introduces much more noises than the single one. We finally report the average results in Table 8.

**Single Node Removal** The black-box GraphToxin demonstrates its superiority when targeting a single node removal. Since we introduce the semantic calibration module, the overall attack performance in the performance-level metrics

is competitive or even superior in the random case, while the overall attack performance in the reconstruction-related metrics declines. A plausible explanation is that the black-box GraphToxin enforces the semantic calibration for full unlearned graph recovery, which might push some nodes cross the model’s decision boundary to obtain the correct prediction but ignore the actual distance in the feature or embedding space. However, the degradation in such metrics remains acceptable.

**Multiple Node Removal** Under the black-box multi-node removal setting, GraphToxin remains superior to all baselines. However, compared to the single-node setting, its overall efficacy in the performance-level metrics declines. In contrast, the attack results of the reconstruction-related metrics are mixed. The performance worsens in PMGK (both cases) and embedding distance (random case) while the attack significantly improves in NRMSE (both cases) and embedding distance (worst case).

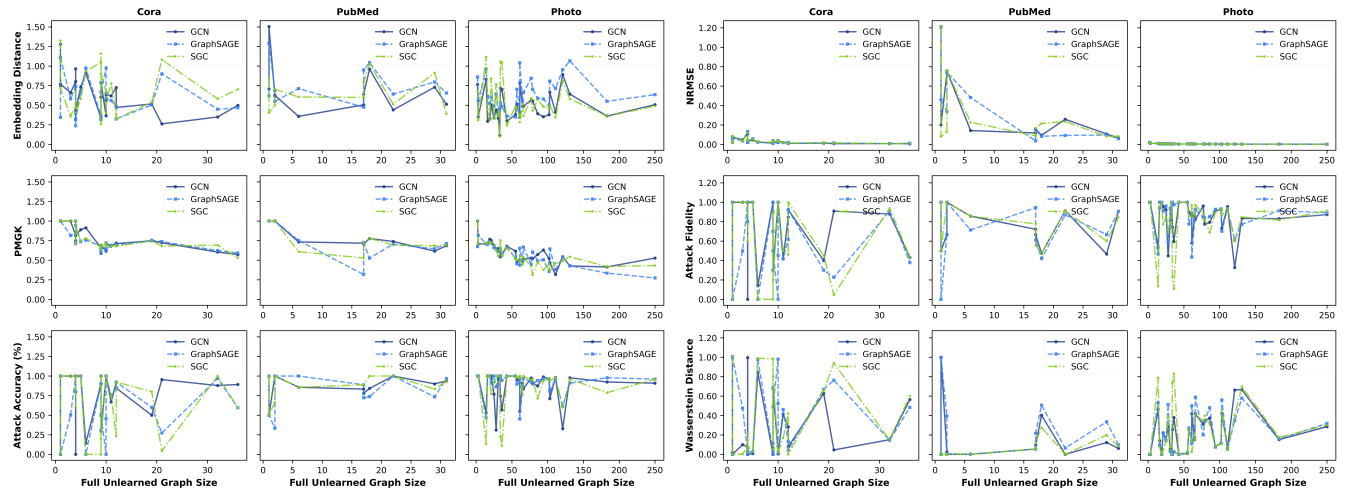


Figure 5: Impact of the Full Unlearned Graph Size

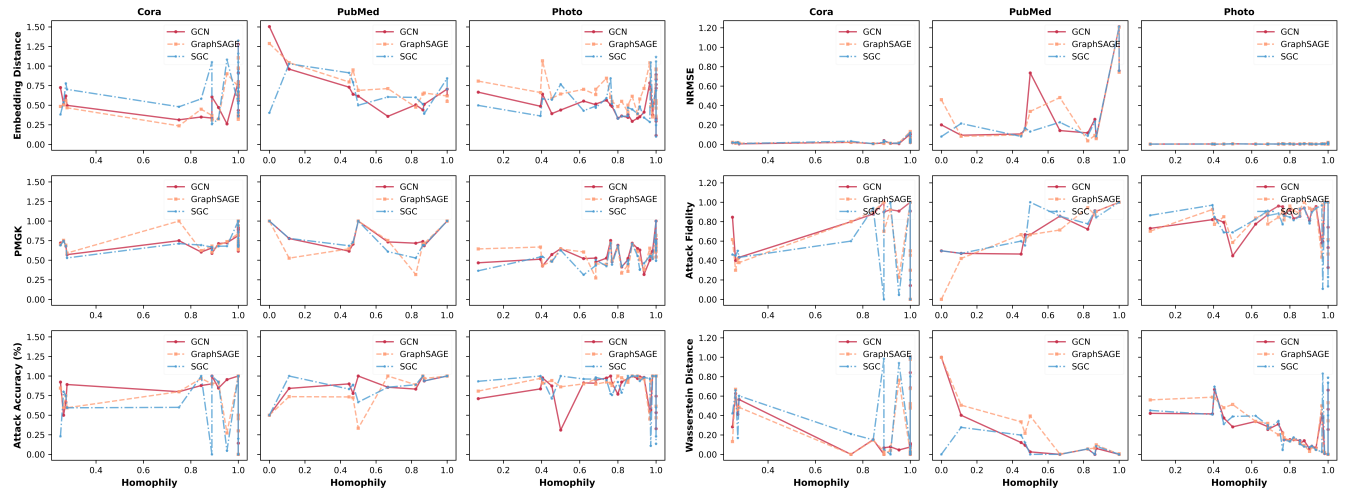


Figure 6: Impact of Node Homophily

TABLE 7: **GraphToxin for Multiple Node Removals Based on Retraining (Backbone: GCN)**. Unit: **1e-2**. Arrow indicates the direction of better performance and the **blue** color denotes the superb ‘best’ results (in **bold**).

Rem. Num	Retraining(ACC/AUC)		Baseline	NRMSE( $\downarrow$ )		ED( $\downarrow$ )		PMGK( $\uparrow$ )		ACC( $\uparrow$ )		FID( $\uparrow$ )		PWD( $\downarrow$ )	
	Random	Worst		Random	Worst	Random	Worst	Random	Worst	Random	Worst	Random	Worst	Random	Worst
5	80.22/96.64	80.30/96.66	Rand. FewE Toxin	2.34	1.71	73.16	73.52	68.01	62.14	27.88	9.94	23.80	8.68	67.08	77.68
				2.13	1.65	61.95	62.41	<b>70.47</b>	60.59	28.75	20.02	28.78	20.15	66.79	72.13
				<b>1.66</b>	<b>1.03</b>	<b>56.27</b>	<b>54.59</b>	70.45	<b>64.82</b>	<b>60.03</b>	<b>70.40</b>	<b>52.06</b>	<b>63.98</b>	<b>47.24</b>	<b>39.08</b>
10	79.98/96.50	80.44/96.49	Rand. FewE Toxin	1.69	1.42	72.50	73.56	58.88	63.76	24.84	17.72	22.04	16.00	66.75	72.57
				1.58	1.31	60.10	59.51	64.65	68.37	24.80	20.54	23.63	17.99	65.72	68.30
				<b>0.99</b>	<b>0.73</b>	<b>54.36</b>	<b>52.29</b>	<b>65.78</b>	<b>68.64</b>	<b>67.83</b>	<b>64.47</b>	<b>59.12</b>	<b>58.99</b>	<b>39.79</b>	<b>44.09</b>
15	79.46/96.57	79.84/96.47	Rand. FewE Toxin	1.41	1.28	73.37	74.06	63.11	62.27	21.28	16.61	19.87	15.21	70.53	75.92
				1.32	1.18	57.73	58.69	<b>70.05</b>	69.47	22.71	17.38	21.82	16.31	67.23	72.32
				<b>0.80</b>	<b>0.69</b>	<b>54.06</b>	<b>55.67</b>	66.05	<b>70.34</b>	<b>65.63</b>	<b>58.79</b>	<b>53.80</b>	<b>53.50</b>	<b>51.01</b>	<b>51.05</b>

TABLE 8: **Black-box GraphToxin for A Single and Multiple Node Removals Based on Retraining.** Unit: **1e-2**. Arrow indicates the direction of better performance and the **blue** color denotes the superb ‘best’ results (in **bold**).

Type	Retraining(ACC/AUC)		Baseline	NRMSE(↓)		ED(↓)		PMGK(↑)		ACC(↑)		FID(↑)		PWD(↓)		
	Random	Worst		Random	Worst	Random	Worst	Random	Worst	Random	Worst	Random	Worst	Random	Worst	
Single	79.66/96.10	79.63/96.09	Toxin	Rand.	11.51	6.29	127.87	120.86	81.09	67.11	12.20	13.85	13.51	14.40	16.19	14.64
				FewE	5.68	3.10	115.91	96.78	<b>82.98</b>	67.97	49.40	65.56	47.62	58.30	11.27	9.25
				<b>4.76</b>	<b>2.49</b>	<b>87.37</b>	<b>80.08</b>	81.56	<b>68.30</b>	<b>72.74</b>	<b>82.07</b>	<b>70.95</b>	<b>73.64</b>	<b>8.28</b>	<b>6.97</b>	
Multiple	79.86/96.09	79.78/96.10	Toxin	Rand.	2.34	1.71	126.49	135.71	65.10	57.04	27.88	9.94	21.81	7.57	14.91	17.83
				FewE	2.35	1.72	111.55	114.68	<b>69.47</b>	59.83	41.92	38.55	33.20	33.63	13.22	12.76
				<b>1.53</b>	<b>1.07</b>	<b>90.04</b>	<b>71.66</b>	67.70	<b>59.93</b>	<b>59.41</b>	<b>69.60</b>	<b>47.88</b>	<b>60.11</b>	<b>11.56</b>	<b>9.63</b>	